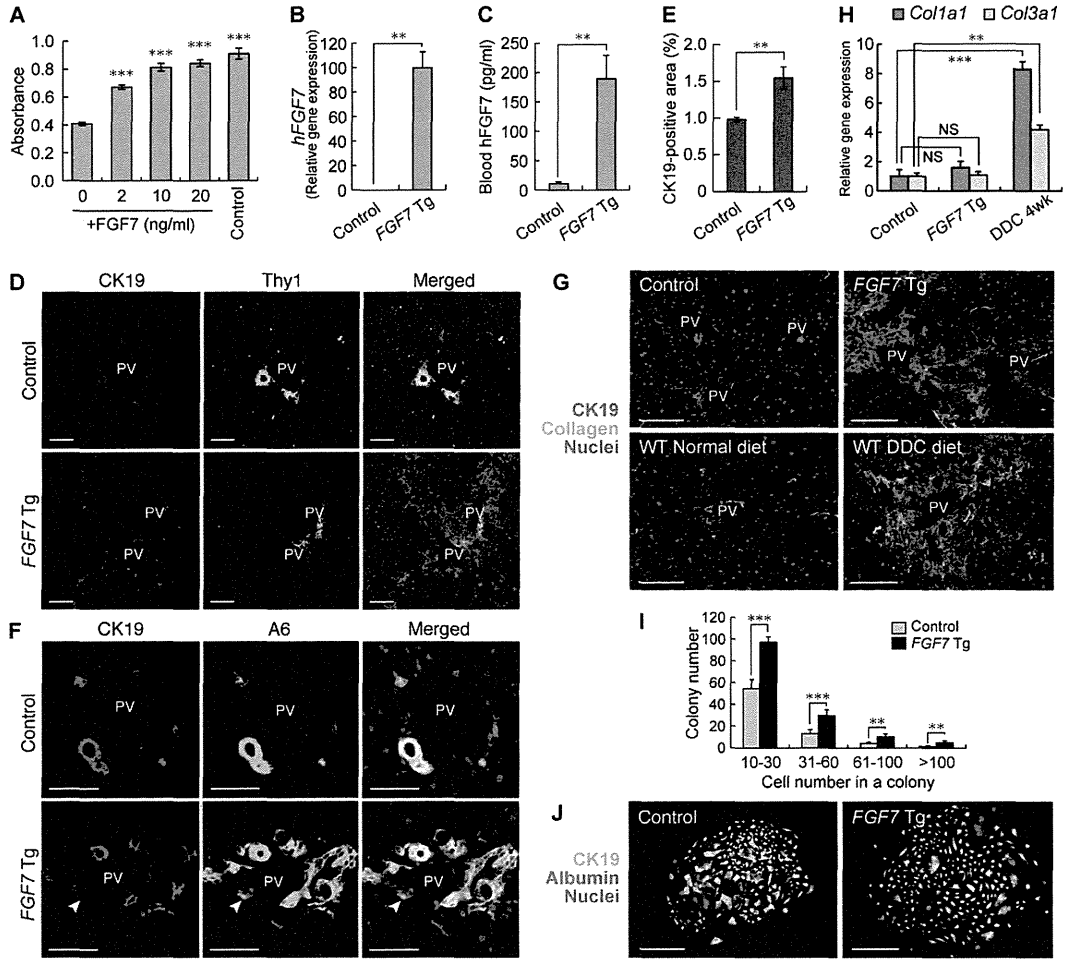

Figure 5. Overexpression of FGF7 can induce the LPC response in the adult mouse liver. (*A*) The level of proliferation of HSCE1 cells was examined by WST-1 assay. Stimulation with epidermal growth factor (EGF) and hepatocyte growth factor (HGF) was used as a control. Mean ± SD (n = 3). (***) $P < 0.001$ compared with no cytokine treatment (0). (*B*) Quantitative RT–PCR analysis was performed to assess human *FGF7* mRNA levels in the liver after 3 wk of Dox administration. Mean ± SE (control, n = 3; Tg, n = 5). (**) $P < 0.01$. (*C*) Serum levels of human FGF7 protein after 3 wk of Dox administration were determined by ELISA. Mean ± SE (control, n = 4; Tg, n = 6). (**) $P < 0.01$. (*D*) Immunostaining of CK19 (red) and Thy1 (green) in the livers of *FGF7* Tg mice and control mice treated with Dox for 4 wk. Bars, 100 μm. (PV) Portal vein. (*E*) Quantitative analysis of CK19-positive areas showed an increased number of LPC-like cells in *FGF7* Tg mice treated with Dox for 4 wk. Mean ± SD (n = 3). (**) $P < 0.01$. (*F*) Immunostaining of CK19 (red) and A6 (green) showed expansion of CK19$^+$ A6$^+$ LPCs in the livers of *FGF7* Tg mice treated with Dox for 4 wk. CK19$^-$ A6$^+$ newly formed hepatocytes were also observed (arrowheads). Bars, 50 μm. (PV) Portal vein. (*G*) Immunostaining of CK19 (red) and collagen (green) in the livers of *FGF7* Tg and control mice, wild-type mice fed a normal diet, and DDC-treated wild-type mice. Bars, 100 μm. (PV) Portal vein. (*H*) Quantitative RT–PCR analysis of *Col1a1* and *Col3a1* mRNA. Mean ± SE (control, n = 3; Tg, n = 5; DDC, n = 3). (**) $P < 0.01$; (***) $P < 0.001$; (NS) not significant. (*I*) EpCAM$^+$ cells were isolated from the livers of *FGF7* Tg mice and control mice 3 wk after Dox treatment and subjected to the in vitro colony formation assay. Mean ± SD (n = 3). (**) $P < 0.01$; (***) $P < 0.001$. (*J*) Immunofluorescence images of representative large colonies stained with anti-CK19 (green) and albumin (red). Bars, 200 μm.

either of these genes at the whole-organ level (Fig. 5H). Thus, overexpression of FGF7 in the liver results in local deposition of ECMs associated with the LPC expansion but does not lead to a global fibrogenic response in the organ.

To further characterize the FGF7-induced LPC-like population in terms of functional criteria, we next performed clonogenic assays to evaluate its proliferative and bilineage differentiation potentials in vitro. It has been well documented that stem/progenitor cell activity of a certain population of liver cells can be defined by their capacity to generate large colonies that are capable of expressing both hepatocyte and BEC lineage markers in culture (Suzuki et al. 2008; Okabe et al. 2009; Dorrell et al. 2011; Shin et al. 2011). When EpCAM$^+$ cells isolated from the *FGF7* Tg mice and the control mice were subjected to in vitro colony formation assays (Okabe et al. 2009), the EpCAM$^+$ cells from the Tg mice formed colonies, including those composed of >100 cells (Fig. 5I). Immunostaining analyses confirmed that these large colonies were composed of both albumin-positive (the hepatocyte marker) and CK19-positive (the LPC/BEC marker)

cells, indicative of the bilineage differentiation in vitro (Fig. 5J). Most importantly, the colony-forming rate for both large and smaller colonies was significantly increased in the *FGF7* Tg mice. Thus, overexpression of FGF7 in vivo in the mouse liver leads to expansion of LPCs that are characterized by LPC marker expressions as well as clonogenicity and bipotency in vitro. Taken together, we conclude that FGF7 alone is sufficient to generate a population of cells that are phenotypically and functionally indistinguishable from LPCs.

Overexpression of FGF7 reverses both the hepatocyte damage and cholestatic liver injury

Given the potent activity of FGF7 in promoting the LPC response, we reasoned that application of this molecule should exert some protective effect on the liver against toxic insults. To test this possibility, the Tg mouse system was used to start ectopic FGF7 expression by Dox administration 1 wk after the onset of the course of DDC-induced chronic liver injury (Fig. 6A). Under this condition, increases in the level of the cholestatic markers TBIL and ALP were greatly reduced in *FGF7* Tg mice compared with the control mice, with the severity of symptoms of jaundice being apparently reduced, which means that bile duct obstruction was alleviated (Fig. 6B,C). At the same time, the levels of AST and ALT were also significantly improved in *FGF7* Tg mice, indicating less hepatocyte injury by overexpression of FGF7 (Fig. 6C). To further substantiate the notion that FGF7 does not simply prevent the damage but rather reverses and improves the symptoms of well-established chronic liver failure, we performed similar experiments by starting Dox administration to induce *FGF7* expression in the liver 3 wk after the onset of the DDC administration (Supplemental Fig. S10A,B). Again, serum biochemical analyses showed decreased levels of both hepatocyte injury and cholestasis markers, although the difference was not statistically significant with regard to ALP (Supplemental Fig. S10C). These data suggest that the severity of the damage on both hepatocytes and BECs can be relieved by an excess of FGF7 through the activation of LPCs that are bipotential and hence capable of contributing to the recovery of both lineages.

Histochemical examination revealed that deposition of brown pigment plugs derived from porphyrin crystals, a hallmark of the DDC-injured liver, was decreased in the Tg liver (Fig. 6D). Single-cell necrosis was reduced in

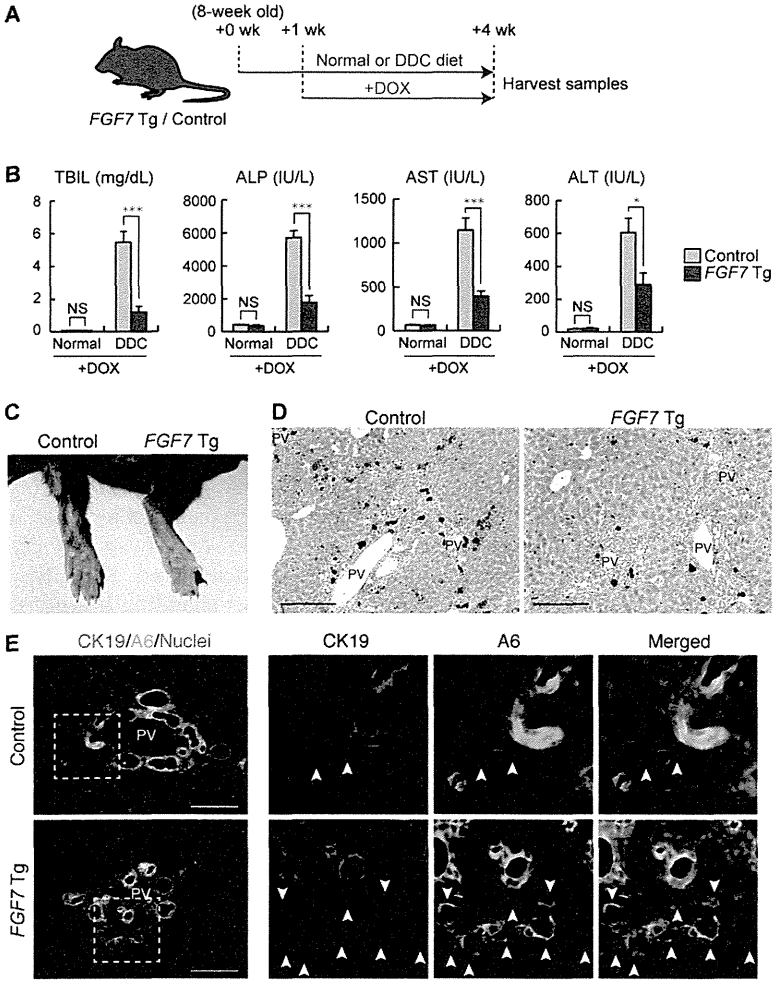

Figure 6. Application of FGF7 improves both the hepatocyte damage and cholestatic liver injury. (*A*) Schematic representation of the experiment. Eight-week-old *FGF7* Tg and control mice were subjected to the DDC-induced liver injury model or left untreated, and 1 wk later, Dox administration was started for FGF7 induction. After 3 wk of treatment, serum and liver samples were harvested for subsequent analyses. (*B*) Serum TBIL, ALP, AST, and ALT levels were measured in control and *FGF7* Tg mice fed a normal (control, $n = 3$; Tg, $n = 3$) or DDC-containing (control, $n = 9$; Tg, $n = 7$) diet. Mean ± SE. (***) $P < 0.001$; (*) $P < 0.05$; (NS) not significant. (*C*) Typical skin color (*right* foot) of the DDC-treated animals at the end of the protocol, indicating that *FGF7* Tg mice suffered less from jaundice than control mice. (*D*) Hematoxylin and eosin staining of livers from DDC-treated animals at the end of the protocol. Bars, 200 μm. (PV) Portal vein. (*E*) Immunostaining of CK19 (red) and A6 (green) in the livers of FGF7 Tg mice and control mice at the end of the protocol. Note that $A6^+$ $CK19^-$ newly formed hepatocytes were increased in the livers of *FGF7* Tg mice. Bars, 100 μm. (PV) Portal vein.

some of the Tg mice compared with the control (data not shown). In the case of the mice fed DDC for 6 wk, some morphological changes associated with the reacting ductules were observed in the Tg mice, including thickened epithelial layers and more dilated luminal structures (Supplemental Fig. S10D,E). Most remarkably, immunostaining analyses revealed that $A6^+$ $CK19^-$ newly formed hepatocytes were dramatically increased around the expanding $A6^+$ $CK19^+$ LPCs (Figs. 6E; Supplemental Fig. S10E). This strongly suggests that overexpression of FGF7 contributes to parenchymal regeneration by accelerating differentiation and production of hepatocytes from LPCs in the DDC-induced liver injury model. In conclusion, our results indicate that FGF7 secreted by $Thy1^+$ cells mediates the activation of adult LPCs as a niche signal and promotes progenitor cell-dependent liver regeneration (Fig. 7).

Discussion

In this study, we demonstrate that FGF7 plays a critical role in inducing LPCs and that the LPC response contributes to survival in severe liver injury. From the standpoint of adult tissue stem/progenitor cells, this study has substantiated the concept of the niche for LPCs in the regenerating liver by molecular characterization.

In general, tissue stem/progenitor cells are supported and regulated by their surrounding microenvironment or the stem cell niche. While several secreted molecules that participate in the LPC response have been reported (Erker and Grompe 2007), their possible involvement as niche signals has not been explored. This study provides compelling evidence that $Thy1^+$ periportal cells form the niche for LPCs by residing in close proximity to LPCs and producing a key regulatory factor, FGF7. Since FGF7-producing $Thy1^+$ cells express markers for portal fibroblasts, hepatic stellate cells, and myofibroblast, we consider that $Thy1^+$ cells are a heterogeneous population of mesenchymal cells. Our data are consistent with a previous report that hepatic stellate cells express FGF7 in chronic liver disease (Steiling et al. 2004). Although further characterization of the $Thy1^+$ cells is needed to give a clear definition of the LPC niche, we hereby propose that the stem cell niche is present in the adult liver under the regenerating conditions. It has been reported that $Thy1^+$ cells are also observed in the livers of patients with fulminant liver failure accompanying the LPC response (Dezso et al. 2007). In addition, high expression of FGF7 in patients with chronic liver diseases (Steiling et al. 2004; Otte et al. 2007) and in experimental rat models of hepatic fibrosis (Murakami et al. 2011) were previously reported. Thus, we predict that LPCs are regulated through the same mechanism in humans as in rodents.

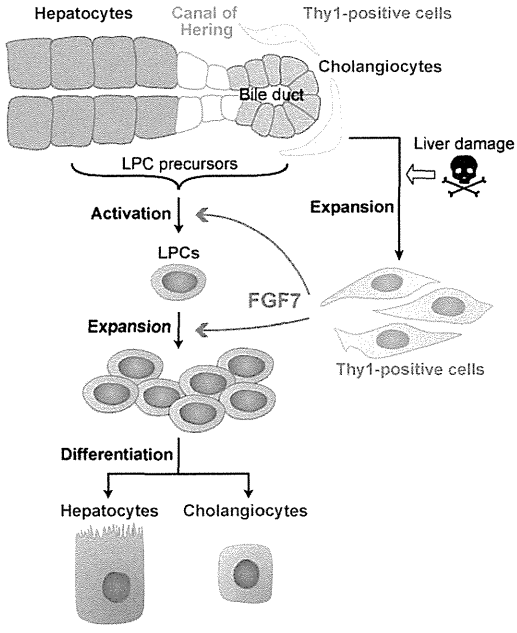

Figure 7. A model for regulatory mechanism of the LPC response by FGF7. In injured livers, $Thy1^+$ mesenchymal cells expand in the periportal area and produce FGF7. FGF7 contributes to liver regeneration by initiating the activation and proliferation of LPCs as the functional niche signal.

The LPC response is a complicated physiological response to liver injuries involving several kinds of cells, such as hepatocytes, BECs, immune cells, hepatic stellate cells, and portal fibroblasts. We demonstrated that FGF7 is both necessary and sufficient for its induction. To our knowledge, this is the first study to prove that FGF signaling is involved in LPC regulation. Upstream and downstream signaling events of FGF7 need to be explored to further elucidate the regulatory mechanism of LPCs. Previous studies have identified TNF (tumor necrosis factor)-like weak inducer of apoptosis (Tweak) as a mitogen for LPCs (Jakubowski et al. 2005; Tirnitz-Parker et al. 2010). Tweak is a member of the TNF family and binds to the FGF-inducible 14-kDa protein (Fn14) receptor (Meighan-Mantha et al. 1999). Although the LPC response in *Fn14* knockout mice was attenuated after 2 wk of CDE treatment, it was restored later and eventually resulted in a level equivalent to that in wild-type mice (Tirnitz-Parker et al. 2010). In contrast, we showed in this study that LPC activation was not sufficiently induced in *Fgf7* knockout mice even after long-term liver injury. Thus, the role of FGF7 signal may be more direct and indispensable in LPC induction, while that of the Tweak/Fn14 pathway may be rather enhancing and not necessarily required. Recently, hepatocyte growth factor (HGF)/c-Met signaling has been reported to play a necessary role in LPC-mediated liver regeneration in the mouse DDC diet model (Ishikawa et al. 2012), although it remains unexplored whether it can also be sufficient to induce the LPC response, as is the case with FGF7. The relationship between FGF7 and these signaling pathways is an important issue to be addressed. In addition, recent studies have suggested that the cellular and molecular mechanisms underlying the injury/regeneration processes in the DDC injury are apparently different from the CDE regimen, another well-appreciated model to study LPCs (Boulter et al. 2012; Español-Suñer et al. 2012). It should be determined whether and how FGF7 is involved in the latter case.

We showed that forced expression of FGF7 in hepatocytes induces the LPC response in the normal liver. Intriguingly, induced LPC-like cells were observed only in the periportal area despite global expression of FGF7 within the liver. As the LPC response upon liver injury also takes place in the periportal region, FGF7-induced LPC-like cells may be derived from the genuine origin and undergo the normal ontogeny of LPCs. The origin of LPCs is still under debate. The canals of Hering that connect bile ducts to hepatocytes have long been considered a promising candidate (Paku et al. 2001); however, direct proof of this idea has been hampered by the lack of a specific molecular marker for these cells. BECs are phenotypically quite similar to LPCs and can thus be a likely candidate (Alison et al. 1996; Okabe et al. 2009). Indeed, recent studies using a genetic lineage tracing system based on *Sox9-CreERT2* mouse lines have suggested this possibility (Dorrell et al. 2011; Furuyama et al. 2011), although the nature of the Sox9-expressing cells should be further evaluated and rigorously determined with considerable caution (Carpentier et al. 2011). At the same time, hepatocytes have also been considered as possible LPC precursors, as they can be converted to BEC- or LPC-like cells under certain circumstances (Michalopoulos et al. 2005; Nishikawa et al. 2005; Zong et al. 2009). With regard to this notion, it should be noted that while FGFR2b is highly expressed in LPCs, it is also weakly but certainly expressed in the hepatocyte fraction. Considering the heterogeneity of hepatocytes, it is worthwhile to explore the nature of LPC precursors based on the expression pattern of FGFR2b. It is also possible that the local environmental cues, such as ECMs, in the periportal region participate in dictating the competence of LPC precursors for activation by FGF7, leading to a spatially stereotyped induction pattern of the LPC response.

While it has long been documented that LPCs appear and proliferate in injured and cancerous livers, whether LPCs participate in regeneration has not been clear to date. Our data, based on loss-of-function and gain-of-function experiments with FGF7, demonstrate that the level of LPC activation correlates with resilience and survival in cases of severe liver injury and suggest that LPCs practically contribute to liver regeneration. It is formally not excluded that FGF7 may act directly on damaged hepatocytes and/or BECs to cause some protective effects, and further analyses will be required to discriminate these possibilities. In either case, FGF7 can be regarded as a highly effective molecule to reverse liver damage. It has been reported that application of recombinant FGF7 protein in mice results in enhanced expression of detoxifying enzymes in the liver, while mice lacking both FGFR1 and FGFR2 in hepatocytes show increased mortality after PHx with impaired expression of those enzymes (Böhm et al. 2010). PHx has generally been regarded as the model for liver regeneration achieved by compensatory proliferation of hepatocytes rather than by LPCs, but several recent studies have implicated a possible involvement of the latter as well (Furuyama et al. 2011; Iverson et al. 2011; Malato et al. 2011). Although the study by Böhm et al. (2010) did not mean to address the role of endogenous FGF7, it would be worth exploring whether the potential beneficial effect of FGF7 observed therein is attributable to ectopic activation of LPCs. An N-terminally truncated form of FGF7, palifermin, has already been approved for the treatment of chemoradiation-induced oral mucositis (Beaven and Shea 2007). In spite of the ability of this drug to improve wound healing responses, its potential for therapeutic application to human liver diseases has not been tested. Our present study provides evidence that FGF7 or its derivatives may have clinical implications for patients with hepatic dysfunction as well.

Materials and methods

Animals

Fgf7 knockout mice (Guo et al. 1996) were obtained from The Jackson Laboratory. All of the experiments in this study were performed on littermates derived from the mating of heterozygotes. In order to generate liver-specific *Tak1*-deficient mice (*Tak1*-LKO mice), mice carrying floxed alleles of the *Tak1* gene ($Tak1^{flox/flox}$) (Sato et al. 2005), maintained by and obtained from JCRB (Japanese Collection of Research Bioresources Cell Bank) Laboratory Animal Resource Bank, NIBIO (National Institute of Biomedical Innovation, Osaka), were crossed with *Alfp-Cre* Tg mice (kindly provided by Dr. Klaus Kaestner, University of Pennsylvania) (Zhang et al. 2005). For the *FGF7* Tg mouse line in which human FGF7 is overexpressed in the liver upon treatment with Dox, the *Alfp-Cre* Tg mice, *ROSA26-rtTA-IRES-EGFP* knock-in mice (obtained from The Jackson Laboratory) (Belteki et al. 2005), and *tetO-CMV-FGF7* Tg mice (kindly provided by Dr. Jeffrey A. Whitsett, Cincinnati Children's Hospital Medical Center) (Tichelaar et al. 2000) were crossed to prepare *Alfp-Cre; rtTA/+; FGF7* triple Tg mice. Littermates lacking the *FGF7* transgene (*Alfp-Cre; rtTA/+*) were used as a control. Dox was administrated in drinking water (2 g/L) supplemented with 1% sucrose. For lineage tracing experiments, the *Alfp-Cre* Tg mice were crossed with the *R26R-EYFP* reporter strain (Srinivas et al. 2001). Wild-type C57BL/6J mice were purchased from CLEA Japan, Inc. All animals were maintained under standard SPF conditions. The experiments were performed according to the guideline set by the institutional animal care and use committee of the University of Tokyo. Mouse LPCs were activated by feeding with a 0.1% DDC-containing diet (F-4643, Bio-serv) or common BDL using a standard technique.

Antibodies

For immunohistochemistry, rat monoclonal antibodies against mouse EpCAM (used at a dilution of 1:200; 552370) and Thy1 (1:200; 553011) were purchased from BD Bioscience. The goat anti-mouse albumin (1:100; A90-234A, Bethyl Laboratories), rabbit anti-Desmin (1:400; ab8592, Abcam), rabbit anti-rat Elastin (1:100; CL55041AP, Cedarlane), rabbit anti-GFP (1:50; G10362, Life Technologies), rabbit anti-human Ki67 (1:200; NCL-Ki67p, Leica), and rabbit anti-Sox9 (1:1000; AB5535, Millipore) antibodies were also commercially obtained and used. A mixture of rabbit anti-collagen type I (1:100; 2150-1410, AbD serotec) and rabbit anti-collagen type III (1:300; ab7778, Abcam) was used to detect collagen fibers. The rat anti-mouse CK19 (TROMA-III) was obtained from the Developmental Studies Hybridoma Bank and used at 250 ng/mL. The rabbit anti-mouse CK19 antibody (1:1000–1:2000) was raised as previously described (Tanimizu

et al. 2003). The rabbit anti-FGF7 (1:100) and anti-FGFR2b (1:200) antibodies were as described (Yamamoto-Fukuda et al. 2003). The A6 antibody (1:10–1:20) was a generous gift from Dr. Valentina Factor (National Institutes of Health). For flow cytometry, the rat anti-EpCAM monoclonal antibody (1:500) was raised as described previously (Okabe et al. 2009). The rat anti-mouse CD45 APC antibody (1:100; 30-F11) was purchased from BD Bioscience. The anti-Thy1 antibody was the same as described above.

Histological analysis

Frozen sections (8 μm) from the liver were placed on APS-coated glass slides (Matsunami Glass) using a HM505E cryostat (Microm International). After blocking in 5% skim milk/PBS, the samples were incubated with primary antibodies and then with fluorescence-conjugated secondary antibodies. Nuclei were counterstained with Hoechst 33342 (Sigma). Liver sections were imaged with fluorescence microscopes (Axioskop 2 plus and Axio Observer.Z1, Zeiss) or a confocal microscope (Fluoview FV1000, Olympus). For the quantification of positive areas, immunostained liver sections were imaged and quantified using an In Cell Analyzer 2000 (GE Healthcare). TUNEL assay was performed using the In Situ Apoptosis Detection kit (MK500, TaKaRa) according to the manufacturer's instructions. Gross pathological and histopathological examinations of *Fgf7* knockout and control mice were performed by BOZO Research Center, Inc.

Section in situ hybridization analysis

Paraffin sections were prepared from liver specimens, and a digoxigenin-labeled antisense RNA probe for mouse *Fgfr2* was used for in situ hybridization by the method of Genostaff, Inc. The probe sequence is shown in Supplemental Table S2, and the hybridization conditions are available on request. After images for in situ hybridization staining were obtained, the sections were further processed for immunohistochemical staining with the anti-CK19 antibody. The same fields of view as in in situ hybridization were chosen and photographed.

Cell preparation and flow cytometry

A single-cell suspension from the liver was obtained by a two-step collagenase perfusion method as described previously (Okabe et al. 2009). In short, liver specimens were perfused with basic perfusion solution containing 0.5 g/L collagenase type IV (Sigma). The undigested clot was redigested with basic perfusion solution containing 0.5 g/L collagenase type IV, 0.5 g/L pronase (Roche), and 50 mg/L DNaseI (Sigma). This digested liver was passed through a 70-μm cell strainer. After centrifugation at 700 rpm for 2 min, the pellet was used for separation of hepatocytes by Percoll density centrifugation. The supernatant was transferred to a new tube and centrifuged repeatedly until no pellet was visible. The final supernatant was centrifuged at 1200 rpm for 5 min, and the precipitated cells were used as NPCs for flow cytometry. Aliquots of cells were blocked with anti-FcR antibody, costained with fluorescence- and/or biotin-conjugated antibodies, and then incubated with PE-conjugated streptavidin (BD Biosciences) if needed. The samples were analyzed by FACSCalibur (Becton Dickinson) or sorted by Moflo XDP (Beckman-Coulter). Dead cells were excluded by propidium iodide staining.

Quantitative RT–PCR

Total RNA was isolated from whole-liver samples or sorted cell populations using Trizol reagent (Invitrogen) and treated with DNaseI (Invitrogen). Total RNA and random hexamer primers were used for cDNA synthesis with SuperScript III (Invitrogen) or High-Capacity cDNA Reverse Transcription kit (Applied Biosystems). Quantitative RT–PCR analyses were performed using LightCycler (Roche) with SYBR Premix Ex Taq (Takara). *Gapdh* was used as an internal control. Primer sequences are listed in Supplemental Table S1.

Cell culture and proliferation assay

The hepatic progenitor cell line HSCE1 was established and characterized as described previously (Okabe et al. 2009). HSCE1 cells were maintained in type I collagen-coated dishes using a medium supplemented with fetal bovine serum and 10 ng/mL each recombinant human EGF and HGF. The proliferative response of HSCE1 cells was examined in the absence of the serum by a colorimetric assay using WST-1 cell proliferation reagent (Roche) according to the manufacturer's directions. The absorbance value (OD450-OD650) was measured using an Emax microplate reader (Molecular Devices).

In vitro colony formation assay

$EpCAM^+$ cells were sorted as described previously (Okabe et al. 2009) and plated at 5×10^3 cells per 35-mm dish. The cells were cultured for 9 d, and then the number and size of colonies were counted.

Human FGF7 immunoassay

Human FGF7 concentration in serum was quantitatively determined in duplicate by FGF7-specific enzyme-linked immunosorbent assay (ELISA; R&D systems, Inc.) according to the manufacturer's instructions. In brief, FGF7 standards and samples were placed in the provided monoclonal antibody-coated microplates. After the reaction, an enzyme-linked polyclonal antibody specific for FGF7 was added and incubated for 2 h at room temperature. The unbound components were washed off at each step, whereas bound FGF7 was determined by ELISA reader (Immunomini NJ2300, Cosmo Bio Co., Ltd.). Statistical analysis in Figure 3H was carried out using a Kruskal-Wallis test and a Mann-Whitney test in SPSS Statistics 17.0 software. The study protocol conformed to the ethical guidelines of the 1975 Declaration of Helsinki and was approved by the ethics committees of Iwate Medical University and The University of Tokyo. Informed consent was obtained from all patients.

Statistical analysis

Data were analyzed and statistics were performed using unpaired two-tailed Student's *t*-test unless otherwise indicated. Comparisons of gene expression in multiple liver cell fractions (Fig. 2D; Supplemental Figs. S4A, S5, S6) were done using one-way analysis of variance (ANOVA) with subsequent Tukey tests. $P < 0.05$ was considered statistically significant.

Acknowledgments

We thank Dr. K. Kaestner, Dr. J.A. Whitsett, and JCRB Laboratory Animal Resource Bank at NIBIO for providing mouse strains; Dr. V. Factor for an antibody; H. Bae, Y. Kamiya, A. Kikuchi, N. Miyata, S. Saito, and H. Sato for technical assistance; and the members of the Miyajima laboratory for discussions and suggestions. The TROMA-III developed by Dr. Rolf Kemler was obtained from the Developmental Studies Hybridoma Bank developed under the auspices of the NICHD and maintained by the Department of Biology at The University of Iowa. This

work was supported by research grants from the Ministry of Education, Culture, Sports, Science, and Technology of Japan (to T.I. and A.M.); Ministry of Health, Labor, and Welfare of Japan (to A.M.); the CREST program from Japan Science and Technology Agency (to A.M.); and the Takeda Science Foundation (to A.M.). H.M.T. was a Research Fellow of the Japan Society for the Promotion of Science.

References

Akhurst B, Croager EJ, Farley-Roche CA, Ong JK, Dumble ML, Knight B, Yeoh GC. 2001. A modified choline-deficient, ethionine-supplemented diet protocol effectively induces oval cells in mouse liver. *Hepatology* **34:** 519–522.

Alison MR, Golding MH, Sarraf CE. 1996. Pluripotential liver stem cells: Facultative stem cells located in the biliary tree. *Cell Prolif* **29:** 373–402.

Alpdogan O, Hubbard VM, Smith OM, Patel N, Lu S, Goldberg GL, Gray DH, Feinman J, Kochman AA, Eng JM, et al. 2006. Keratinocyte growth factor (KGF) is required for postnatal thymic regeneration. *Blood* **107:** 2453–2460.

Beaven AW, Shea TC. 2007. The effect of palifermin on chemotherapyand radiation therapy-induced mucositis: A review of the current literature. *Support Cancer Ther* **4:** 188–197.

Beer HD, Bittner M, Niklaus G, Munding C, Max N, Goppelt A, Werner S. 2005. The fibroblast growth factor binding protein is a novel interaction partner of FGF-7, FGF-10 and FGF-22 and regulates FGF activity: Implications for epithelial repair. *Oncogene* **24:** 5269–5277.

Belteki G, Haigh J, Kabacs N, Haigh K, Sison K, Costantini F, Whitsett J, Quaggin SE, Nagy A. 2005. Conditional and inducible transgene expression in mice through the combinatorial use of Cre-mediated recombination and tetracycline induction. *Nucleic Acids Res* **33:** e51.

Bettermann K, Vucur M, Haybaeck J, Koppe C, Janssen J, Heymann F, Weber A, Weiskirchen R, Liedtke C, Gassler N, et al. 2010. TAK1 suppresses a NEMO-dependent but NF-κB-independent pathway to liver cancer. *Cancer Cell* **17:** 481–496.

Bird TG, Lorenzini S, Forbes SJ. 2008. Activation of stem cells in hepatic diseases. *Cell Tissue Res* **331:** 283–300.

Böhm F, Speicher T, Hellerbrand C, Dickson C, Partanen JM, Ornitz DM, Werner S. 2010. FGF receptors 1 and 2 control chemically induced injury and compound detoxification in regenerating livers of mice. *Gastroenterology* **139:** 1385–1396.

Boulter L, Govaere O, Bird TG, Radulescu S, Ramachandran P, Pellicoro A, Ridgway RA, Seo SS, Spee B, Van Rooijen N, et al. 2012. Macrophage-derived Wnt opposes Notch signaling to specify hepatic progenitor cell fate in chronic liver disease. *Nat Med* **18:** 572–579.

Carpentier R, Suñer RE, van Hul N, Kopp JL, Beaudry JB, Cordi S, Antoniou A, Raynaud P, Lepreux S, Jacquemin P, et al. 2011. Embryonic ductal plate cells give rise to cholangiocytes, periportal hepatocytes, and adult liver progenitor cells. *Gastroenterology* **141:** 1432–1438.

Dezso K, Jelnes P, Laszlo V, Baghy K, Bodor C, Paku S, Tygstrup N, Bisgaard HC, Nagy P. 2007. Thy-1 is expressed in hepatic myofibroblasts and not oval cells in stem cell-mediated liver regeneration. *Am J Pathol* **171:** 1529–1537.

Dorrell C, Erker L, Schug J, Kopp JL, Canaday PS, Fox AJ, Smirnova O, Duncan AW, Finegold MJ, Sander M, et al. 2011. Prospective isolation of a bipotential clonogenic liver progenitor cell in adult mice. *Genes Dev* **25:** 1193–1203.

Duncan AW, Dorrell C, Grompe M. 2009. Stem cells and liver regeneration. *Gastroenterology* **137:** 466–481.

Engelhardt NV, Factor VM, Yasova AK, Poltoranina VS, Baranov VN, Lasareva MN. 1990. Common antigens of mouse oval and biliary epithelial cells. Expression on newly formed hepatocytes. *Differentiation* **45:** 29–37.

Erker L, Grompe M. 2007. Signaling networks in hepatic oval cell activation. *Stem Cell Res* **1:** 90–102.

Español-Suñer R, Carpentier R, Van Hul N, Legry V, Achouri Y, Cordi S, Jacquemin P, Lemaigre F, Leclercq IA. 2012. Liver progenitor cells yield functional hepatocytes in response to chronic liver injury in mice. *Gastroenterology* **143:** 1564–1575.

Farber E. 1956. Similarities in the sequence of early histological changes induced in the liver of the rat by ethionine, 2-acetylamino-fluorene, and 3′-methyl-4-dimethylaminoazobenzene. *Cancer Res* **16:** 142–148.

Fausto N. 2004. Liver regeneration and repair: Hepatocytes, progenitor cells, and stem cells. *Hepatology* **39:** 1477–1487.

Furuyama K, Kawaguchi Y, Akiyama H, Horiguchi M, Kodama S, Kuhara T, Hosokawa S, Elbahrawy A, Soeda T, Koizumi M, et al. 2011. Continuous cell supply from a Sox9-expressing progenitor zone in adult liver, exocrine pancreas and intestine. *Nat Genet* **43:** 34–41.

Gerhart J. 1999. 1998 Warkany lecture: Signaling pathways in development. *Teratology* **60:** 226–239.

Guo L, Degenstein L, Fuchs E. 1996. Keratinocyte growth factor is required for hair development but not for wound healing. *Genes Dev* **10:** 165–175.

Inokuchi S, Aoyama T, Miura K, Osterreicher CH, Kodama Y, Miyai K, Akira S, Brenner DA, Seki E. 2010. Disruption of TAK1 in hepatocytes causes hepatic injury, inflammation, fibrosis, and carcinogenesis. *Proc Natl Acad Sci* **107:** 844–849.

Ishikawa T, Factor VM, Marquardt JU, Raggi C, Seo D, Kitade M, Conner EA, Thorgeirsson SS. 2012. Hepatocyte growth factor/c-met signaling is required for stem-cell-mediated liver regeneration in mice. *Hepatology* **55:** 1215–1226.

Itoh N, Ornitz DM. 2008. Functional evolutionary history of the mouse Fgf gene family. *Dev Dyn* **237:** 18–27.

Iverson SV, Comstock KM, Kundert JA, Schmidt EE. 2011. Contributions of new hepatocyte lineages to liver growth, maintenance, and regeneration in mice. *Hepatology* **54:** 655–663.

Jakubowski A, Ambrose C, Parr M, Lincecum JM, Wang MZ, Zheng TS, Browning B, Michaelson JS, Baetscher M, Wang B, et al. 2005. TWEAK induces liver progenitor cell proliferation. *J Clin Invest* **115:** 2330–2340.

Knight B, Matthews VB, Olynyk JK, Yeoh GC. 2005. Jekyll and Hyde: Evolving perspectives on the function and potential of the adult liver progenitor (oval) cell. *Bioessays* **27:** 1192–1202.

Knight B, Akhurst B, Matthews VB, Ruddell RG, Ramm GA, Abraham LJ, Olynyk JK, Yeoh GC. 2007. Attenuated liver progenitor (oval) cell and fibrogenic responses to the choline deficient, ethionine supplemented diet in the BALB/c inbred strain of mice. *J Hepatol* **46:** 134–141.

Lee CH, Javed D, Althaus AL, Parent JM, Umemori H. 2012. Neurogenesis is enhanced and mossy fiber sprouting arises in FGF7-deficient mice during development. *Mol Cell Neurosci* **51:** 61–67.

Libbrecht L, Roskams T. 2002. Hepatic progenitor cells in human liver diseases. *Semin Cell Dev Biol* **13:** 389–396.

Liu XH, Aigner A, Wellstein A, Ray PE. 2001. Up-regulation of a fibroblast growth factor binding protein in children with renal diseases. *Kidney Int* **59:** 1717–1728.

Lowes KN, Brennan BA, Yeoh GC, Olynyk JK. 1999. Oval cell numbers in human chronic liver diseases are directly related to disease severity. *Am J Pathol* **154:** 537–541.

Lu J, Izvolsky KI, Qian J, Cardoso WV. 2005. Identification of FGF10 targets in the embryonic lung epithelium during bud morphogenesis. *J Biol Chem* **280:** 4834–4841.

Malato Y, Naqvi S, Schürmann N, Ng R, Wang B, Zape J, Kay MA, Grimm D, Willenbring H. 2011. Fate tracing of mature hepatocytes in mouse liver homeostasis and regeneration. *J Clin Invest* **121:** 4850–4860.

Meighan-Mantha RL, Hsu DK, Guo Y, Brown SA, Feng SL, Peifley KA, Alberts GF, Copeland NG, Gilbert DJ, Jenkins NA, et al. 1999. The mitogen-inducible Fn14 gene encodes a type I transmembrane protein that modulates fibroblast adhesion and migration. *J Biol Chem* **274:** 33166–33176.

Michalopoulos GK, DeFrances MC. 1997. Liver regeneration. *Science* **276:** 60–66.

Michalopoulos GK, Barua L, Bowen WC. 2005. Transdifferentiation of rat hepatocytes into biliary cells after bile duct ligation and toxic biliary injury. *Hepatology* **41:** 535–544.

Murakami KI, Kaji T, Shimono R, Hayashida Y, Matsufuji H, Tsuyama S, Maezono R, Kosai KI, Takamatsu H. 2011. Therapeutic effects of vitamin A on experimental cholestatic rats with hepatic fibrosis. *Pediatr Surg Int* **27:** 863–870.

Nishikawa Y, Doi Y, Watanabe H, Tokairin T, Omori Y, Su M, Yoshioka T, Enomoto K. 2005. Transdifferentiation of mature rat hepatocytes into bile duct-like cells in vitro. *Am J Pathol* **166:** 1077–1088.

Okabe M, Tsukahara Y, Tanaka M, Suzuki K, Saito S, Kamiya Y, Tsujimura T, Nakamura K, Miyajima A. 2009. Potential hepatic stem cells reside in $EpCAM^+$ cells of normal and injured mouse liver. *Development* **136:** 1951–1960.

Otte JM, Schwenger M, Brunke G, Schmitz F, Otte C, Kiehne K, Kloehn S, Monig H, Schmidt WE, Herzig KH. 2007. Differential regulated expression of keratinocyte growth factor and its receptor in experimental and human liver fibrosis. *Regul Pept* **144:** 82–90.

Paku S, Schnur J, Nagy P, Thorgeirsson SS. 2001. Origin and structural evolution of the early proliferating oval cells in rat liver. *Am J Pathol* **158:** 1313–1323.

Ponder KP. 1996. Analysis of liver development, regeneration, and carcinogenesis by genetic marking studies. *FASEB J* **10:** 673–682.

Preisegger KH, Factor VM, Fuchsbichler A, Stumptner C, Denk H, Thorgeirsson SS. 1999. Atypical ductular proliferation and its inhibition by transforming growth factor β1 in the 3,5-diethoxycarbonyl-1,4-dihydrocollidine mouse model for chronic alcoholic liver disease. *Lab Invest* **79:** 103–109.

Qiao J, Uzzo R, Obara-Ishihara T, Degenstein L, Fuchs E, Herzlinger D. 1999. FGF-7 modulates ureteric bud growth and nephron number in the developing kidney. *Development* **126:** 547–554.

Sato S, Sanjo H, Takeda K, Ninomiya-Tsuji J, Yamamoto M, Kawai T, Matsumoto K, Takeuchi O, Akira S. 2005. Essential function for the kinase TAK1 in innate and adaptive immune responses. *Nat Immunol* **6:** 1087–1095.

Shin S, Walton G, Aoki R, Brondell K, Schug J, Fox A, Smirnova O, Dorrell C, Erker L, Chu AS, et al. 2011. Foxl1-Cre-marked adult hepatic progenitors have clonogenic and bilineage differentiation potential. *Genes Dev* **25:** 1185–1192.

Srinivas S, Watanabe T, Lin CS, William CM, Tanabe Y, Jessell TM, Costantini F. 2001. Cre reporter strains produced by targeted insertion of EYFP and ECFP into the ROSA26 locus. *BMC Dev Biol* **1:** 4.

Steiling H, Werner S. 2003. Fibroblast growth factors: Key players in epithelial morphogenesis, repair and cytoprotection. *Curr Opin Biotechnol* **14:** 533–537.

Steiling H, Muhlbauer M, Bataille F, Scholmerich J, Werner S, Hellerbrand C. 2004. Activated hepatic stellate cells express keratinocyte growth factor in chronic liver disease. *Am J Pathol* **165:** 1233–1241.

Strick-Marchand H, Masse GX, Weiss MC, Di Santo JP. 2008. Lymphocytes support oval cell-dependent liver regeneration. *J Immunol* **181:** 2764–2771.

Suzuki A, Sekiya S, Onishi M, Oshima N, Kiyonari H, Nakauchi H, Taniguchi H. 2008. Flow cytometric isolation and clonal identification of self-renewing bipotent hepatic progenitor cells in adult mouse liver. *Hepatology* **48:** 1964–1978.

Tanimizu N, Miyajima A. 2007. Molecular mechanism of liver development and regeneration. *Int Rev Cytol* **259:** 1–48.

Tanimizu N, Nishikawa M, Saito H, Tsujimura T, Miyajima A. 2003. Isolation of hepatoblasts based on the expression of Dlk/Pref-1. *J Cell Sci* **116:** 1775–1786.

Terauchi A, Johnson-Venkatesh EM, Toth AB, Javed D, Sutton MA, Umemori H. 2010. Distinct FGFs promote differentiation of excitatory and inhibitory synapses. *Nature* **465:** 783–787.

Tichelaar JW, Lu W, Whitsett JA. 2000. Conditional expression of fibroblast growth factor-7 in the developing and mature lung. *J Biol Chem* **275:** 11858–11864.

Tirnitz-Parker JE, Viebahn CS, Jakubowski A, Klopcic BR, Olynyk JK, Yeoh GC, Knight B. 2010. Tumor necrosis factor-like weak inducer of apoptosis is a mitogen for liver progenitor cells. *Hepatology* **52:** 291–302.

Turanyi E, Dezso K, Csomor J, Schaff Z, Paku S, Nagy P. 2010. Immunohistochemical classification of ductular reactions in human liver. *Histopathology* **57:** 607–614.

Turner N, Grose R. 2010. Fibroblast growth factor signalling: From development to cancer. *Nat Rev Cancer* **10:** 116–129.

Yamamoto-Fukuda T, Aoki D, Hishikawa Y, Kobayashi T, Takahashi H, Koji T. 2003. Possible involvement of keratinocyte growth factor and its receptor in enhanced epithelial-cell proliferation and acquired recurrence of middle-ear cholesteatoma. *Lab Invest* **83:** 123–136.

Yanger K, Stanger BZ. 2011. Facultative stem cells in liver and pancreas: Fact and fancy. *Dev Dyn* **240:** 521–529.

Yovchev MI, Zhang J, Neufeld DS, Grozdanov PN, Dabeva MD. 2009. Thymus cell antigen-1-expressing cells in the oval cell compartment. *Hepatology* **50:** 601–611.

Zhang L, Rubins NE, Ahima RS, Greenbaum LE, Kaestner KH. 2005. Foxa2 integrates the transcriptional response of the hepatocyte to fasting. *Cell Metab* **2:** 141–148.

Zong Y, Panikkar A, Xu J, Antoniou A, Raynaud P, Lemaigre F, Stanger BZ. 2009. Notch signaling controls liver development by regulating biliary differentiation. *Development* **136:** 1727–1739.

Biochemical and Biophysical Research Communications 430 (2013) 751–756

Contents lists available at SciVerse ScienceDirect

Biochemical and Biophysical Research Communications

journal homepage: www.elsevier.com/locate/ybbrc

Nephronectin is upregulated in acute and chronic hepatitis and aggravates liver injury by recruiting CD4 positive cells

Fuyuki F. Inagaki [a,b], Minoru Tanaka [a], Natsuko F. Inagaki [a], Tomoki Yagai [a], Yuya Sato [c], Kiyotoshi Sekiguchi [c], Naoki Oyaizu [d], Norihiro Kokudo [b], Atsushi Miyajima [a,*]

[a] Institute of Molecular and Cellular Biosciences, The University of Tokyo, Tokyo, Japan
[b] Hepato-Billary-Pancreatic Surgery Division, Artificial Organ and Transplantation Division, Department of Surgery, Graduate School of Medicine, The University of Tokyo, Tokyo, Japan
[c] Institute for Protein Research, Osaka University, Osaka, Japan
[d] Department of Laboratory Medicine, Research Hospital, Institute of Medical Science, The University of Tokyo, Tokyo, Japan

ARTICLE INFO

Article history:
Received 9 November 2012
Available online 1 December 2012

Keywords:
Liver
Acute hepatitis
Chronic hepatitis
Nephronectin

ABSTRACT

Nephronectin (Npnt) is an extracellular matrix protein known to play a critical role in kidney development; however, its physiological role in the liver remains elusive. Here we show that Npnt expression is upregulated in mouse models of both acute and chronic hepatitis induced by Concanavalin A (Con A) and 3,5-diethocarbonyl-1,4-dihydrocollidine (DDC), respectively. In both models, Npnt was localized in inflammatory foci and was mainly secreted from mesenchymal cells and in part by cholangiocytes. Interestingly, ectopic expression of Npnt in hepatocytes induced the development of granuloma-like cell clusters mainly composed of $CD4^+$ T cells or NKT cells but did not induce apparent hepatitis. Furthermore, we found that Npnt exacerbated the Con A-induced acute hepatitis. These results indicate that Npnt plays an important role in the initiation of hepatitis by recruiting $CD4^+$ T cells or NKT cells into the foci of inflammation. In addition, we reveal that Npnt expression is also upregulated in human hepatitis. Therefore, Npnt may be a potential therapeutic target for acute and chronic hepatitis.

1. Introduction

Previously we performed a microarray analysis of cholangiocytes derived from a normal liver and 3,5-diethoxycarbonyl-1,4-dihydro-collidine (DDC)-induced chronic hepatitis liver [1]. We found that the expression of about 50 genes was significantly upregulated in chronic hepatitis liver. Most genes were related to fibrosis, epithelial-mesenchymal transition, hepatic stem/progenitor cell response. Among these genes, *Nephronectin* (*Npnt*) was expressed 5-fold higher in DDC-induced chronic hepatitis liver than in normal liver.

Npnt is an extracellular matirix (ECM) protein, containing an Arg-Gly-Asp (RGD) motif. ECMs are mesh structures composed of proteins and carbohydrates, filling intercellular spaces. The interaction of ECM with cell surface integrins plays crucial roles in development, immunity, inflammation, and homeostasis by regulating cell adhesion, migration, growth, differentiation, and apoptosis [2–4]. The binding of integrin to ECM depends on an RGD motif in ECM proteins [5,6]. The RGD motif is the cell recognition site involved in various ECMs and platelet adhesion proteins, such as fibronectin, vitronectin, osteopontin (OPN), and Npnt [7–10]. Among them, OPN is known to exacerbate hepatitis [11–13].

Although Npnt has been known to play an important role in kidney development [14,15], its functions in the liver remain unknown. Considering that both Npnt and OPN contain an RGD motif and that OPN is a key modulator in hepatitis, it is anticipated that Npnt may also play some roles in liver inflammation. Here we elucidate the roles of Npnt in hepatitis.

2. Materials and methods

See Supplementary materials and methods for more details.

Abbreviations: Npnt, nephronectin; OPN, osteopontin; Con A, concanavalin A; DDC, 3,5-diethoxycarbonyl-1,4-dihydro-collidine; NKT, natural killer T cells; BD, bile duct; PV, portal vein; CV, central vein; ECM, extracellular matrix; HTVi, hydrodynamic tail vein injection; PC, parenchymal cell; CK19, cytokeratin 19; Thy1, thymocyte differentiation antigen 1; EpCAM, epithelial cell adhesion molecule; AST, aspartate amino transferase; ALT, alanine transaminase; RGD, arginine–glycine–aspartate; SCID, severe combined immunodeficiency.

* Corresponding author. Address: Institute of Molecular and Cellular Biosciences, The University of Tokyo, 1-1-1 Yayoi, Bunkyo-ku, Tokyo 113-0032, Japan. Fax: +81 3 5841 8475.

E-mail addresses: inagaki-tky@umin.ac.jp (F.F. Inagaki), tanaka@iam.u-tokyo.ac.jp (M. Tanaka), n_inagaki@iam.u-tokyo.ac.jp (N.F. Inagaki), 4956218042@mail.ecc.u-tokyo.ac.jp (T. Yagai), y.sato@protein.osaka-u.ac.jp (Y. Sato), sekiguch@protein.osaka-u.ac.jp (K. Sekiguchi), oyaizu@ims.u-tokyo.ac.jp (N. Oyaizu), kokudo-2su@h.u-tokyo.ac.jp (N. Kokudo), miyajima@iam.u-tokyo.ac.jp (A. Miyajima).

0006-291X/$ - see front matter © 2012 Elsevier Inc. All rights reserved.
http://dx.doi.org/10.1016/j.bbrc.2012.11.076

2.1. Animals

Specific pathogen-free male C57BL/6J mice and FOX CHASE SCID mice were purchased from Nihon CLEA (Tokyo, Japan). All experimental procedures in this study were approved by the Institutional Animal Care and Use Committee of the University of Tokyo (approval number is 24003).

2.2. Con A-induced acute hepatitis and DDC-induced chronic hepatitis

Concanavalin A (Con A) was purchased from Sigma–Aldrich (St. Louis, MO) and was injected intravenously into mice through the tail vein. The dose of Con A was 20 mg/kg or 15 mg/kg. A diet containing 0.1% 3,5-diethoxycarbonyl-1,4-dihydro-collidine (DDC) was purchased from Nihon CLEA (Tokyo, Japan).

2.3. Overexpression by hydrodynamic tail vein injection (HTVi) method

Mouse Npnt cDNA was amplified by PCR (primers (5′ – 3′): GCTAGCGCAGCTGGCTTTCTTCGAGGC and CTCGAGGCTCAAGCCAGAGCCAATGGC) and was inserted into the NheI and XhoI sites of a pLIVE vector (Mirus, Madison, WI). pLIVE-Npnt (50 μg) was diluted with TransIT-EE Hydrodynamic Delivery Solution (Mirus, Madison, WI) and injected into the tail vein of 7-week-old male C57BL/6 mice. pLIVE-SEAP (secreted alkaline phosphatase) (50 μg) was used as a control. One week after injection, mice were sacrificed for histological analysis.

2.4. Statistical analysis

Student's *t*-tests with equal variance and two-tailed distribution were used to determine the significance of differences between two groups (Excel statistical analysis software, Microsoft Japan, Tokyo, Japan). A *P*-value of 0.05 or lower was considered significant. Results where indicated are expressed as mean ± standard error.

3. Results

3.1. Expression of Npnt in mice hepatitis models

To investigate the correlation of Npnt expression with hepatitis, we examined Npnt mRNA levels in both the acute hepatitis model induced by Con A administration and the chronic hepatitis model induced by DDC diet (Fig. 1A and B) [16,17]. Npnt expression was rapidly induced at 12 h and decreased gradually thereafter in Con A-induced acute hepatitis. While, in chronic hepatitis, Npnt expression levels increased 2 weeks after feeding of DDC diet. These results suggested that Npnt expression correlated with the severity of hepatitis. Immunohistochemistry (IHC) also revealed that Npnt was strongly expressed in areas around portal veins, bile ducts, and central veins in Con A-induced acute hepatitis livers, while it was weakly expressed in areas around portal veins and central veins in normal livers (Fig. 1C–F). Strong expression of Npnt was also observed in the livers of DDC-induced chronic hepatitis in

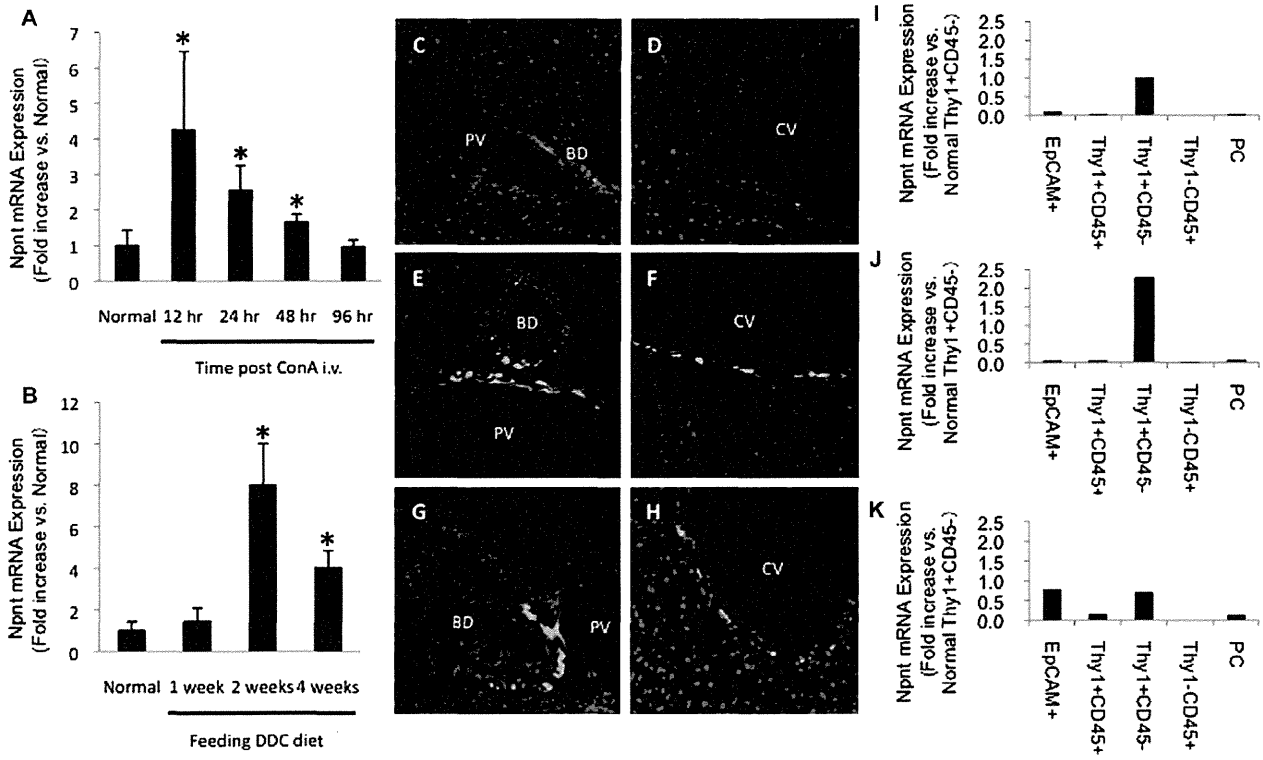

Fig. 1. Npnt expression in normal, acute and chronic hepatitis livers and identification of liver cells expressing Npnt. (A, B) Expression of mouse liver Npnt mRNA was analyzed in Con A-induced acute liver injury (A) and DDC-induced chronic liver injury (B). Con A (20 mg/kg) was injected into mice intravenously. The fold increase of Npnt mRNA in injured livers relative to normal livers is shown. Beta-actin mRNA was used as an internal control. $n = 5$ per group. $^*p < 0.05$. (C–H) IHC of Npnt in a normal liver (C, D), acute hepatitis liver 12 h after intravenous injection of Con A (20 mg/kg) (E, F), and chronic hepatitis liver 2 weeks after feeding of the DDC diet (G, H). Liver sections were immunostained with anti-Npnt antibody (green). Nuclei were counterstained with Hoechst (blue). Original magnification, 200×. PV: portal vein, BD: bile duct, CV: central vein (I–K) Analyses of Npnt mRNA expression in various types of cells from a normal liver (I), acute hepatitis liver 12 h after Con A (20 mg/kg) injection (J), and chronic hepatitis liver 2 weeks after feeding of the DDC diet (K). Each type of cell was isolated from livers based on the expression of EpCAM, Thy1, and CD45 by a cell sorter.

areas similar to acute hepatitis, especially around portal veins and bile ducts (Fig. 1G and H).

Inflammatory liver diseases are known to be accompanied by an increase in the number of neutrophils, NKT cells, and T cells [18,19]. Histological examinations consistently showed the infiltration of blood cells into periportal and pericentral areas in Con A-induced acute hepatitis livers, whereas a few blood cells were detected in normal livers (Supplementary Fig. 1A and B). Livers in DDC-induced chronic hepatitis exhibited a marked infiltration of blood cells into the periportal area (Supplementary Fig. 1C). These results raise the possibility of a close relationship between the infiltration of blood cells and expression of Npnt in both acute and chronic hepatitis.

3.2. Identification of Npnt-producing cells

In order to identify Npnt-producing cells, we isolated intrahepatic cell components from normal, acute and chronic hepatitis liver, respectively. We sorted 5 cell populations; EpCAM$^+$, EpCAM$^-$ Thy1$^+$ CD45$^+$, EpCAM$^-$ Thy1$^+$ CD45$^-$, EpCAM$^-$ Thy1$^-$ CD45$^+$, and parenchymal cells (PC), which correspond to cholangiocytes, T lymphocytes, mesenchymal cells (fibroblast and/or myofibroblast), hematopoietic cells except for T lymphocytes, and hepatocytes, respectively. Npnt was expressed only in mesenchymal cells in normal liver (Fig. 1I) and increased in Con A-induced hepatitis (Fig. 1J). Immunostaining revealed that Thy1$^+$ mesenchymal cells around portal and central veins were more abundant in Con A-induced hepatitis liver compared to normal liver (Supplementary Fig. 2A and B). In the DDC-fed liver, Npnt was mainly expressed in mesenchymal cells and cholangiocytes (Fig. 1K) and the number of cholangiocytes and mesenchymal cells increased markedly compared to that in normal liver (Supplementary Fig. 2A and C).

3.3. Overexpression of Npnt in liver induces granuloma-like cell clusters

To reveal the physiological role of Npnt in the liver, we ectopically expressed Npnt in livers using the hydrodynamic tail vein injection (HTVi) method. This is a simple method to achieve hepatocyte-specific gene expression by injecting expression vectors with a large amount of buffer, into the mice tail vein and is suitable for assessment of *in vivo* function of secreted proteins [20,21]. Histological examination showed that granuloma-like cell clusters developed in livers expressing Npnt (Fig. 2A and B), whereas such clusters were not found in livers that received the control plasmid vector (Fig. 2C). Granuloma-like cell clusters (White arrow) are formed around Npnt positive area (Fig. 2E and F), suggesting that Npnt plays an important role in the recruitment of immune cells.

It should be noted that upregulation of Npnt expression and infiltration of blood cells were observed in the two hepatitis models (Supplementary Fig. 1). In general, granulomas are mainly comprised of macrophages, neutrophils, and lymphocytes. Interestingly, Npnt overexpression by HTVi in SCID mice did not induce the formation of granuloma-like cell clusters (Fig. 2D). Because SCID mice lack T cells, B cells, and NKT cells, the clusters of cells recruited by Npnt overexpression in C57BL/6 mice are likely

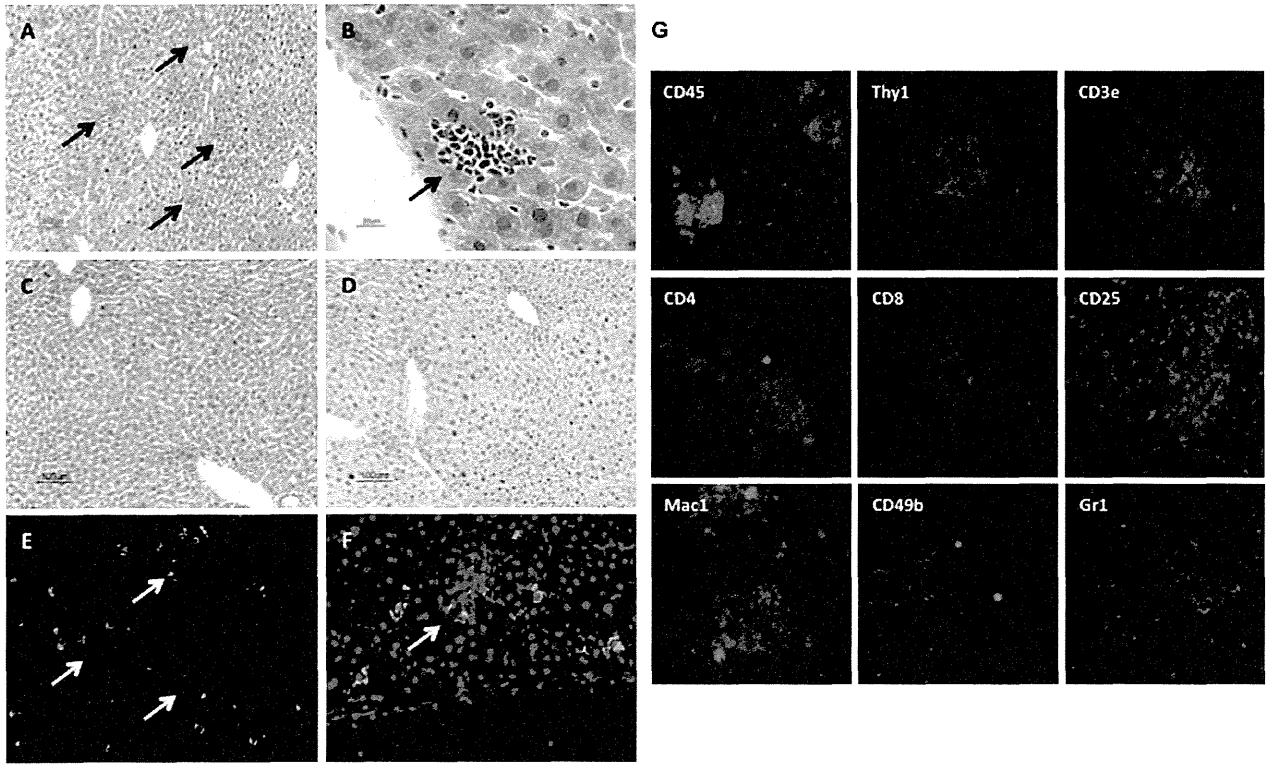

Fig. 2. *In vivo* overexpression of Npnt induces granuloma-like cell cluster formation. (A–D) Histological analysis of mouse livers overexpressing Npnt or SEAP (used as control). (A, B) C57BL/6J mice were analyzed 1 week after HTVi of pLIVE-Npnt. (C) C57BL/6J mice were analyzed 1 week after HTVi of pLIVE-SEAP. (D) SCID mice were analyzed 1 week after HTVi of pLIVE-Npnt. Granuloma-like cell clusters (black arrow) are observed only in Npnt overexpressing C57BL/6J mice. Sections were stained with hematoxylin and eosin. Original magnification, 100× (A, C and D) and 400× (B). (E, F) IHC of Npnt in Npnt overexpressing liver. Npnt producing hepatocytes and secreted Npnt are stained green. Granuloma-like cell clusters (white arrow) are formed around highly-concentrated area of secreted Npnt. Original magnification, 100× (E) and 400× (F). (G) IHC of granuloma-like cell clusters by various cell surface markers in C57BL/6J mice after HTVi of pLIVE-Npnt plasmid. Liver sections were stained with anti-CD45, Thy1, CD3e, CD4, CD8, CD25, Mac1, CD49b, Gr1 antibody, respectively (magenta), and nuclei were counterstained with Hoechst (blue). Original magnification, 400×.

to be composed of these immune cells, consistent with recent reports that the numbers of NKT cells and T cells were increased in inflammatory liver disease such as Con A-induced hepatitis [18,19].

3.4. Characterization of blood cells recruited by Npnt

We next characterized the immune cells forming granuloma-like cell clusters in livers expressing Npnt. Immunostaining of liver sections with several cell surface markers revealed that the cells forming granuloma-like clusters were almost all positive for CD45, Thy1, and CD3e. $CD4^+$, $Mac1^+$ and $CD49b^+$ cells were included in some cell clusters, whereas none of the clusters examined contained $CD8^+$, $CD25^+$ and $Gr1^+$ cells (Fig. 2G). These results suggested that Npnt recruited either $CD4^+$ T cells or NKT cells.

3.5. Overexpression of Npnt exacerbates Con A-induced acute hepatitis

It is known that NKT cells and T cells play a critical role in hepatitis including the Con A-induced acute hepatitis model, while the depletion of liver NK cells fails to inhibit Con A-induced hepatic injury [22]. It should be noted that overexpression of Npnt in livers induced the formation of granuloma-like cell clusters consisting of $CD4^+$ T cells or NKT cells, but did not augment liver injury as measured by serum markers such as AST and ALT (data not shown). These results suggest that Npnt plays a crucial role in the recruitment of immune cells to inflammatory foci, but does not activate the recruited cells, raising the possibility that Npnt may be mainly involved in the initial step of the pathogenesis of hepatitis and that $CD4^+$ T cells or NKT cells recruited to inflammatory foci are activated by other stimuli such as inflammatory cytokines.

In order to investigate the effect of Npnt in hepatitis, we injected Con A (15 mg/kg) intravenously into mice seven days after HTVi of Npnt expression or control vector. In control mice, the severity of liver damage, as reflected by serum AST and ALT levels, peaked at 12 h and then declined 72 h after Con A injection. In contrast, mice injected with the Npnt expression vector exhibited more severe liver injury with a time course similar to that in control mice (Fig. 3A and B). These data suggested that $CD4^+$ T cells or NKT cells recruited by Npnt are involved in liver injury by the activation of their cytotoxicity.

3.6. The RGD motif is responsible for the formation of granuloma-like cell clusters

The RGD motif has been known to be a prerequisite for the integrin binding activity of Npnt [9,10]. In order to reveal whether the interaction between integrin and Npnt is responsible for the formation of granuloma-like cell clusters or not, we constructed an Npnt mutant lacking the RGD motif (Fig. 3C middle) and expressed

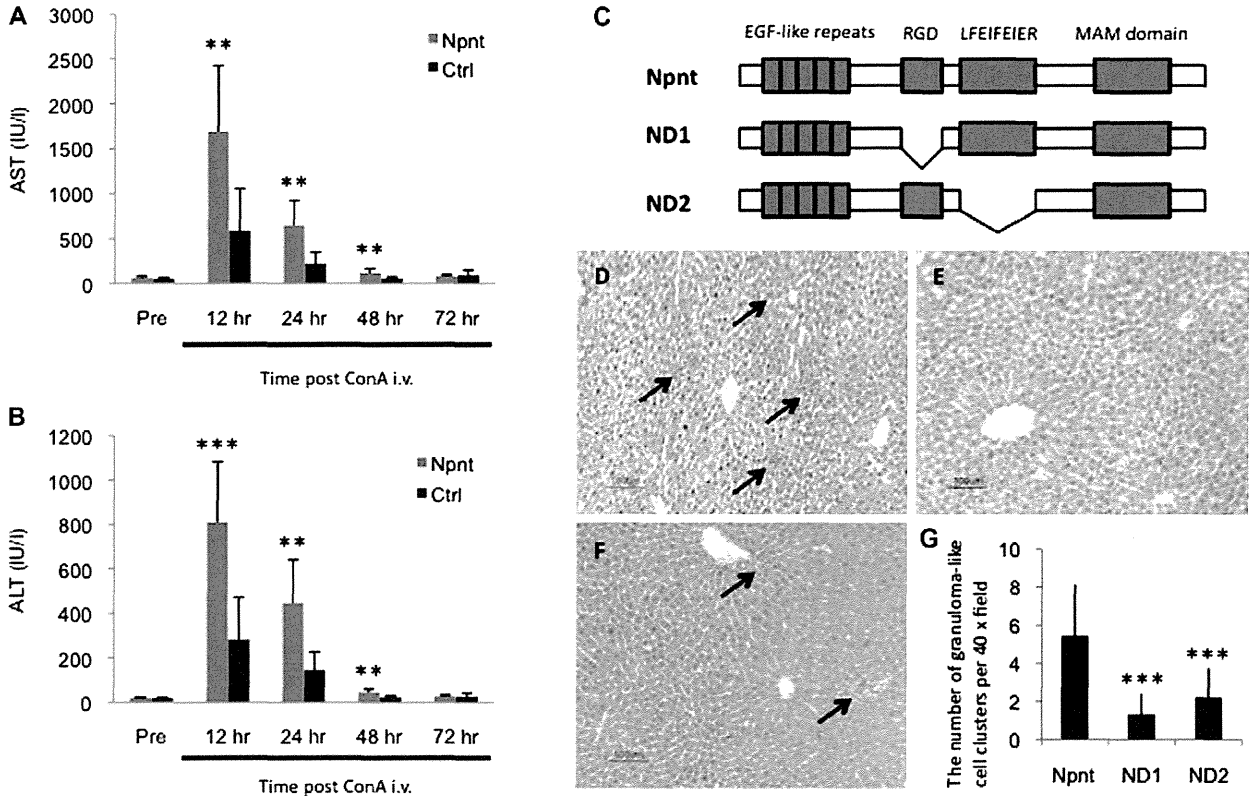

Fig. 3. *In vivo* overexpression of Npnt exacerbates Con A-induced acute hepatitis and RGD motif is necessary for the formation of granuloma-like cell clusters. Plasma aspartate aminotransferase (AST) levels (U/L) (A) and plasma alanine aminotransferase (ALT) levels (U/L) (B) were analyzed in pLIVE-SEAP (Ctrl vector) HTVi or pLIVE-Npnt HTVi mice at 0 (Pre), 12, 24, 48 and 72 h after intravenous injection of Con A (15 mg/kg). $n = 6$ (Ctrl), 5 (Npnt HTVi) per time point. $^{**}p \leq 0.01$, $^{***}p \leq 0.001$ vs. Ctrl vector HTVi group. (C) Schematic of wild type Npnt (top: Npnt), RGD deletion mutant (middle: ND1), and LFEIFEIER deletion mutant (lower: ND2). (D–F) Representative histology of livers. Livers of C57BL/6J mice were analyzed 1 week after injection of pLIVE-Npnt (wild type) (D), pLIVE-Npnt RGD deletion mutant (E), or pLIVE-Npnt LFEIFEIER deletion mutant (F) plasmids by HTVi. Sections were stained with hematoxylin and eosin. Granuloma-like cell clusters are observed (black arrow). Original magnification, 100×. (G) Quantification of granuloma-like clusters. The average number of granuloma-like clusters per 40× field of view is shown. Twenty-five random fields from 5 mice per group were used for analysis. $^{***}p \leq 0.001$ vs. native form of Npnt.

it in the liver by HTVi method. The number of granuloma-like cell clusters for the deletion mutant in livers was significantly lower than that for the native form of Npnt (Fig. 3D, E and G). Sato et al. reported that the LFEIFEIER sequence at the C-terminal side of the RGD motif plays a supportive role in high-affinity binding to α8β1 integrin [23]. We therefore constructed a deletion mutant lacking the LFEIFEIER sequence (Fig. 3C lower) and expressed it in the liver by HTVi method. The deletion mutant induced the formation of granuloma-like cell clusters at an intermediate level between the native form of Npnt and the RGD deletion mutant (Fig. 3D, F and G). These results strongly suggested that the RGD motif mediated the recruitment of $CD4^+$ T cells or NKT cells and that the LFEIFEIER sequence partly contributed to the recruitment.

3.7. Expression of Npnt in human livers

To examine the possibility that Npnt is involved in human hepatitis, we investigated Npnt expression in human liver specimens. In normal livers, Npnt was weakly expressed in periportal areas (Fig. 4A and B). In contrast, Npnt was strongly and extensively expressed in periportal fibrotic areas of chronic hepatitis livers where the infiltration of numerous immune cells was observed (Fig. 4C and D). These data indicate that Npnt is upregulated and involved in the pathogenesis of hepatitis in humans as well as mice.

4. Discussion

In this study, we have investigated the pathogenic role of Npnt in liver injury. The expression of Npnt mRNA was transiently upregulated in our mouse models of acute and chronic hepatitis. In Con A-induced acute hepatitis, inflammatory foci were found in the portal area and around the central vein [24]. In this model, Npnt-expressing cells were $Thy1^+CD45^-$ cells, possibly mesenchymal cells, in periportal and pericentral areas. On the other hand, in DDC-induced chronic hepatitis, also known as cholangitis, inflammatory foci were observed within Glisson's capsules, especially around bile ducts [17]. In this model, Npnt expressing cells were $Thy1^+CD45^-$ cells and $EpCAM^+$ cholangiocytes. In both injury models, Npnt expressing cells were clearly increased and localized in inflammatory foci. Overexpression of Npnt by the HTVi method induced the development of granuloma-like cell clusters in the parenchymal area of the liver. Since plasmid DNA is mainly introduced into hepatocytes by HTVi, it is suggested that the ectopic expression of Npnt in hepatocytes contributes to the recruitment of immune cells and formation of cell clusters in the parenchymal area. IHC revealed that granuloma-like cell clusters consist of cells of the T cell lineage ($Thy1^+$ $CD3e^+$ $CD4^{+/-}$ $CD8^-$ $CD25^-$ $Mac1^{+/-}$ $CD49b^{+/-}$), mainly $CD4^+$ T cells and NKT cells, as the latters are $CD49b^+$ and partially $CD4^+$ and $Mac1^+$ [25,26]. A previous study using T cell-deficient mice and T cell depletion with specific antibodies revealed that Con A-induced liver injury was mediated by $CD4^+$ T cells [27,28]. In addition, Takeda et al. [29] reported that CD1d knockout mice lacking NKT cells were resistant to Con A, indicating a role for NKT cells in acute hepatitis. Consistently, overexpression of Npnt by HTVi in SCID mice, which lack T cells, B cells, and NKT cells, failed to induce granuloma-like cell clusters, indicating that these cells are involved in the development of granuloma-like cell clusters. Furthermore we showed that $CD4^+$ T cells and NKT cells were recruited by the interaction of cell surface integrin and the RGD motif.

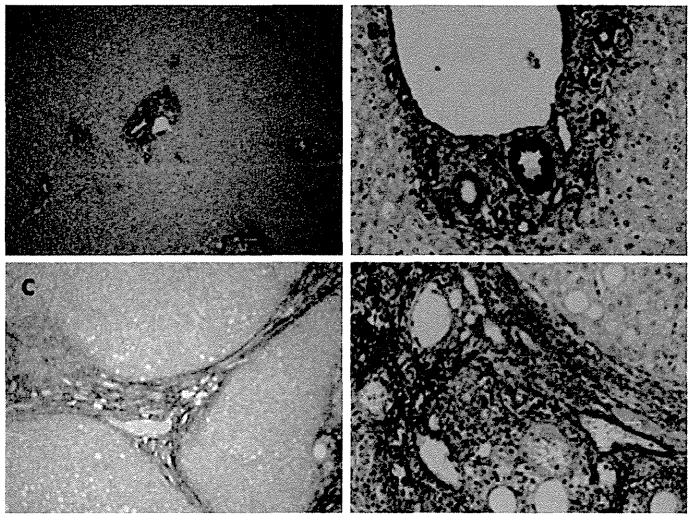

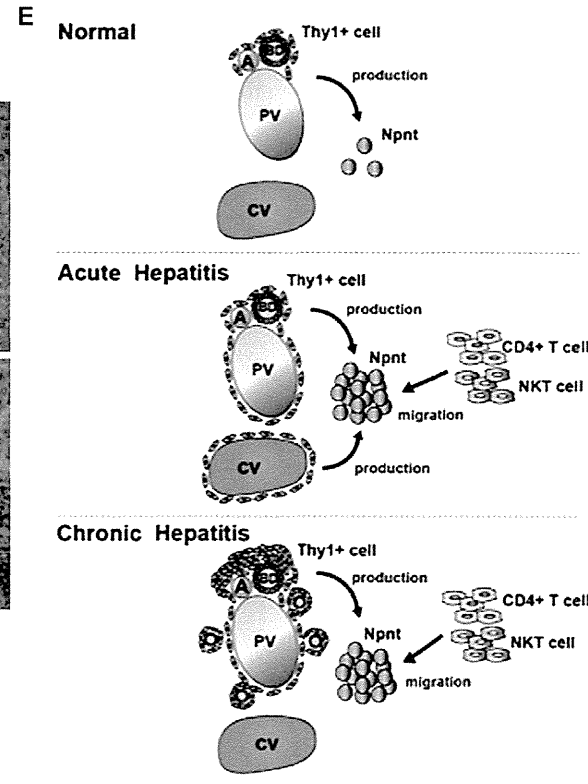

Fig. 4. Npnt expression in human liver sections and a model of the Npnt role in hepatitis. (A–D) Npnt immunostaining of normal (A, B) and cirrhotic (C, D) human liver tissue. Color was developed using metal enhanced diaminobenzidine as a substrate. Counterstaining was performed with hematoxylin. Original magnifications, 50× (A, C); 200× (B, D). (E) In a normal liver, $Thy1^+$ cells produce a small amount of Npnt. In Con A-induced acute hepatitis, $Thy1^+$ cells proliferate in both periportal and pericentral areas and produce a large amount of Npnt. In DDC-induced chronic hepatitis, the outgrowth of bile ducts and surrounding stromal tissue is induced in the portal area. In addition to $Thy1^+$ cells, cholangiocytes produce Npnt. In both cases, secreted Npnt promotes the migration of NKT cells and $CD4^+$ T cells and these cells finally contribute to the exacerbation of hepatitis. PV: portal vein, BD: bile duct, A: hepatic artery, CV: central vein.

Con A-activated NKT cells are known to secrete osteopontin (OPN), another matrix protein containing the RGD motif [11]. However, the mechanism of recruiting NKT cells into the inflammatory foci in injured liver has remained unknown. Our study revealed that Npnt played a crucial role for recruiting $CD4^+$ T cells or NKT cells into the liver and tethering them in inflammatory foci. Furthermore, Npnt expression by HTVi exacerbated Con A-induced acute hepatitis. These results suggest the synergistic action of Npnt, OPN, and Con A for the recuitment and activation of NKT cells, which also explains why the administration of non-peptide mimetics of the RGD motif ameliorates Con A-induced liver injury [30].

In summary, our study revealed the pathogenic role of Npnt in hepatitis as shown in Fig. 4E. In normal livers, mesenchymal cells produce a small amount of Npnt to maintain the immune system around portal veins in livers. In Con A-induced acute hepatitis, mesenchymal cells proliferate in periportal and pericentral areas and produce a large amount of Npnt. In DDC-induced chronic hepatitis, bile ducts together with the surrounding stromal tissue proliferate and cholangiocytes, in addition to mesenchymal cells, produce Npnt, leading to cholangitis. In both cases, Npnt promotes the infiltration of $CD4^+$ T cells or NKT cells via an interaction between the RGD motif and integrin. This is the first report showing the role of Npnt in hepatitis via the recruitment of $CD4^+$ T cells or NKT cells. NKT cells also secrete OPN, contributing to the progression of hepatitis as described previously [11]. Since Npnt knockout mice display renal agenesis or kidney hypoplasia at birth and are lethal, further investigation using conditional knockout mice would help us better understand the roles of Npnt in liver diseases. Because mouse and human Npnt share 88% sequence homology [31], functions of Npnt may be conserved in human and we, in fact, showed that Npnt was expressed more extensively in human chronic hepatitis livers than in normal livers. It would be interesting to study whether the expression level of Npnt is correlated with the severity of hepatitis or the prognosis of patients. While further clinical studies to confirm our present findings are necessary, Npnt may become a potential therapeutic target for acute and chronic hepatitis.

Conflict of interest

The authors declare no financial or commercial conflict of interest.

Acknowledgments

We would like to thank Dr. Tohru Ito for providing us with the pLIVE-SEAP vector and Ms. Naoko Miyata for the excellent cell sorting. This work was supported in part by research grants from the Ministry of Education, Culture, Sports, Science, and Technology of Japan, Ministry of Health, Labour, and Welfare of Japan, the CREST program of the Japan Science and Technology Agency, and the Takeda Science Foundation.

Appendix A. Supplementary data

Supplementary data associated with this article can be found, in the online version, at http://dx.doi.org/10.1016/j.bbrc.2012.11.076.

References

[1] M. Okabe, Y. Tsukahara, M. Tanaka, et al., Potential hepatic stem cells reside in EpCAM+ cells of normal and injured mouse liver, Development 136 (2009) 1951–1960.
[2] E. Ruoslahti, M.D. Pierschbacher, New perspectives in cell adhesion: RGD and integrins, Science 238 (1987) 491–497.
[3] S.B. Carter, Principles of cell motility: the direction of cell movement and cancer invasion, Nature 208 (1965) 1183–1187.
[4] I.U. Ali, R.O. Hynes, Effects of LETS glycoprotein on cell motility, Cell 14 (1978) 439–446.
[5] X.P. Du, E.F. Plow, A.L. Frelinger 3rd, et al., Ligands "activate" integrin alpha IIb beta 3 (Platelet GPIIb-IIIa), Cell 65 (1991) 409–416.
[6] A.L. Frelinger 3rd, X.P. Du, E.F. Plow, et al., Monoclonal antibodies to ligand-occupied conformers of integrin alpha IIb beta 3 (glycoprotein IIb-IIIa) alter receptor affinity, specificity, and function, J. Biol. Chem. 266 (1991) 17106–17111.
[7] L.M. Schnapp, N. Hatch, D.M. Ramos, et al., The human integrin alpha 8 beta 1 functions as a receptor for tenascin, fibronectin, and vitronectin, J. Biol. Chem. 270 (1995) 23196–23202.
[8] S. Denda, L.F. Reichardt, U. Müller, Identification of osteopontin as a novel ligand for the integrin alpha8 beta1 and potential roles for this integrin-ligand interaction in kidney morphogenesis, Mol. Biol. Cell 9 (1998) 1425–1435.
[9] R. Brandenberger, A. Schmidt, J. Linton, et al., Identification and characterization of a novel extracellular matrix protein nephronectin that is associated with integrin alpha8beta1 in the embryonic kidney, J. Cell Biol. 154 (2001) 447–458.
[10] N. Morimura, Y. Tezuka, N. Watanabe, et al., Molecular cloning of POEM: a novel adhesion molecule that interacts with alpha8beta1 integrin, J. Biol. Chem. 276 (2001) 42172–42181.
[11] H. Diao, S. Kon, K. Iwabuchi, et al., Osteopontin as a mediator of NKT cell function in T cell-mediated liver diseases, Immunity 21 (2004) 539–550.
[12] R. Kawashima, S. Mochida, A. Matsui, et al., Expression of osteopontin in Kupffer cells and hepatic macrophages and Stellate cells in rat liver after carbon tetrachloride intoxication: a possible factor for macrophage migration into hepatic necrotic areas, Biochem. Biophys. Res. Commun. 256 (1999) 527–531.
[13] Y. Wang, S. Mochida, R. Kawashima, et al., Increased expression of osteopontin in activated Kupffer cells and hepatic macrophages during macrophage migration in Propionibacterium acnes-treated rat liver, J. Gastroenterol. 35 (2000) 696–701.
[14] J.H. Miner, Mystery solved: discovery of a novel integrin ligand in the developing kidney, J. Cell Biol. 154 (2001) 257–259.
[15] J.M. Linton, G.R. Martin, L.F. Reichardt, The ECM protein nephronectin promotes kidney development via integrin alpha8beta1-mediated stimulation of Gdnf expression, Development 134 (2007) 2501–2509.
[16] T.M. Rahman, H.J. Hodgson, Animal models of acute hepatic failure, Int. J. Exp. Pathol. 81 (2000) 145–157.
[17] P. Fickert, U. Stöger, A. Fuchsbichler, et al., A new xenobiotic-induced mouse model of sclerosing cholangitis and biliary fibrosis, Am. J. Pathol. 171 (2007) 525–536.
[18] H. Fujii, S. Seki, S. Kobayashi, et al., A murine model of NKT cell-mediated liver injury induced by alpha-galactosylceramide/d-galactosamine, Virchows Arch. 446 (2005) 663–673.
[19] R. Zhu, S. Diem, L.M. Araujo, et al., The Pro-Th1 cytokine IL-12 enhances IL-4 production by invariant NKT cells: relevance for T cell-mediated hepatitis, J. Immunol. 178 (2007) 5435–5442.
[20] G. Zhang, V. Budker, J.A. Wolff, High levels of foreign gene expression in hepatocytes after tail vein injections of naked plasmid DNA, Hum. Gene Ther. 10 (1999) 1735–1737.
[21] G. Zhang, X. Gao, Y.K. Song, et al., Hydroporation as the mechanism of hydrodynamic delivery, Gene Ther. 11 (2004) 675–682.
[22] S. Toyabe, S. Seki, T. Iiai, et al., Requirement of IL-4 and liver NK1+ T cells for concanavalin A-induced hepatic injury in mice, J. Immunol. 159 (1997) 1537–1542.
[23] Y. Sato, T. Uemura, K. Morimitsu, et al., Molecular basis of the recognition of nephronectin by integrin alpha8beta1, J. Biol. Chem. 284 (2009) 14524–14536.
[24] H. Mizuhara, E. O'Neill, N. Seki, et al., T cell activation-associated hepatic injury: mediation by tumor necrosis factors and protection by interleukin 6, J. Exp. Med. 179 (1994) 1529–1537.
[25] T. Kawano, J. Cui, Y. Koezuka, et al., CD1d-restricted and TCR-mediated activation of valpha14 NKT cells by glycosylceramides, Science 278 (1997) 1626–1629.
[26] J. Cui, T. Shin, T. Kawano, et al., Requirement for Valpha14 NKT cells in IL-12-mediated rejection of tumors, Science 278 (1997) 1623–1626.
[27] Z. Dong, H. Wei, R. Sun, et al., The roles of innate immune cells in liver injury and regeneration, Cell. Mol. Immunol. 4 (2007) 241–252.
[28] G. Tiegs, J. Hentschel, A. Wendel, A T cell-dependent experimental liver injury in mice inducible by concanavalin A, J. Clin. Invest. 90 (1992) 196–203.
[29] K. Takeda, Y. Hayakawa, L. Van Kaer, et al., Critical contribution of liver natural killer T cells to a murine model of hepatitis, Proc. Natl. Acad. Sci. USA 97 (2000) 5498–5503.
[30] R. Hershkoviz, O. Lider, R. Bruck, et al., Treatment of immune cell-mediated liver damage by nonpeptidic mimetics of the extracellular matrix-associated Arg-Gly-Asp epitope, J. Hepatol. 22 (1995) 158–164.
[31] J.T. Huang, V. Lee, Identification and characterization of a novel human nephronectin gene in silico, Int. J. Mol. Med. 15 (2005) 719–724.

THE JOURNAL OF BIOLOGICAL CHEMISTRY VOL. 287, NO. 34, pp. 28586–28597, August 17, 2012

α1- and α5-containing Laminins Regulate the Development of Bile Ducts via β1 Integrin Signals*[S]

Received for publication, February 6, 2012, and in revised form, June 24, 2012 Published, JBC Papers in Press, July 3, 2012, DOI 10.1074/jbc.M112.350488

Naoki Tanimizu[‡§1], **Yamato Kikkawa**[¶], **Toshihiro Mitaka**[‡], **and Atsushi Miyajima**[§]

From the [‡]*Department of Tissue Development and Regeneration, Research Institute for Frontier Medicine, Sapporo Medical University School of Medicine, S-1, W-17, Chuo-ku, Sapporo, 060-8556, Japan,* [¶]*Laboratory of Clinical Biochemistry, Tokyo University of Pharmacy and Life Sciences, Hachioji 192-0392, Japan, and* [§]*Institute of Molecular and Cellular Biosciences, The University of Tokyo, 1-1-1 Yayoi, Bunkyo-ku, Tokyo, 113-0032, Japan*

Background: Laminin isoforms are suggested to differentially regulate epithelial morphogenesis.
Results: Liver epithelial cells could not establish apicobasal polarity without laminin α1 or β1 integrin signal, whereas they formed immature lumen structures without laminin α5.
Conclusion: Laminins α1 and α5 are necessary to start and complete epithelial morphogenesis, respectively, during bile duct development.
Significance: Laminins α1 and α5 sequentially regulate different developmental processes to form epithelial tissues.

Signals derived from basal lamina components are important for developing three-dimensional architecture of epithelial tissues. Laminins consisting of α, β, and γ subunits in basal lamina play pivotal roles in the formation and maintenance of epithelial tissue structures. However, it remains unclear which laminin isoforms transmit signals and how epithelial cells receive them to regulate multiple developmental processes. In three-dimensional culture of a liver progenitor cell line, Hepatic Progenitor Cells Proliferating on Laminin (HPPL), the cells establish apicobasal polarity and form cysts with a central lumen. Neutralizing antibody against β1 integrin blocked the formation and maintenance of the cyst structure, indicating that β1 integrin signaling was necessary throughout the morphogenesis. Although the addition of α1-containing laminin, a ligand of β1 integrin, induced cyst formation, it was dispensable for the maintenance of the cyst, suggesting that HPPL produces another ligand for β1 integrin to maintain the structure. Indeed, we found that HPPL produced α5-containing laminin, and siRNA against laminin α5 partially inhibited the lumen formation. In fetal liver, p75NTR$^+$ periportal fibroblasts and bile duct epithelial cells, known as cholangiocytes, expressed α1- and α5-containing laminins, respectively. In laminin α5 KO liver, cholangiocytes normally emerged, but the number of bile ducts was decreased. These results suggest that α1-containing laminin is sufficient as a component of the basal lamina for the commitment of bipotential liver progenitors to cholangiocytes and the apicobasal polarization, whereas α5-containing laminin is necessary for the formation of mature duct structures. Thus, α1- and α5-containing laminins differentially regulate the sequential events to form epithelial tissues via β1 integrin signals.

Epithelial organs such as the lung, pancreas, kidney, and liver contain tissue structures such as acini, glands, and tubules to perform the functions of each organ. Epithelial apicobasal polarity in these tissue structures is essential for the directional transport of nutritional and metabolic substances in the liver, absorption of water and ions in the kidney, and gas exchange in the lung. The liver has two epithelial tissue structures, hepatic cords and bile ducts. Cholangiocytes, the epithelial cellular components of bile ducts, differentiate from hepatoblasts, bipotential liver progenitor cells, in midgestation and form tubular structures in the perinatal period (1, 2). Cholangiocytes first form ductal plates, epithelial cell layers around the portal vein, that are then reorganized into bile duct tubules. Recent studies revealed that the apical membrane is established at the early stage of bile duct morphogenesis (3, 4). Because abnormal development or degeneration of the apical lumina of bile ducts results in cholestasis that leads to liver failure (5), the formation and maintenance of the luminal space are crucial for performing the physiological roles of bile ducts.

Intracellular signals from either the apical or basal side of epithelial cells affect the formation and/or maintenance of the luminal structure of epithelial tissues. Cdc42 and phosphatase and tensin homolog on chromosome 10 (PTEN) are localized at the apical domain and segregate the apical domain in the plasma membrane to generate the apical lumen (6, 7). On the other hand, epithelial cells receive signals from extracellular matrix (ECM)[2] proteins on the basal side.

A major functional component in basal lamina is a laminin heterotrimer consisting of α, β, and γ chains (8, 9). Until now, five α, four β, and three γ chains, which are assembled into 18 different laminin isoforms, have been identified in mammals (10). Laminin isoforms are expressed differentially in a spatiotemporal manner and play substantial roles in the development of epithelial structures and functions (9). The expression of laminin isoforms in the normal and regenerating liver has been extensively studied (11, 12). In normal mouse and human adult

* This work was supported by a research grant from the Ministry of Education, Culture, Sports, Science, and Technology, Japan (to N. T., A. M., and T. M.).
[S] This article contains supplemental Figs. 1–7 and Movies 1 and 2.
[1] To whom correspondence should be addressed. Tel.: 81-11-611-2111 (ext. 2391); Fax: 81-11-615-3099; E-mail: tanimizu@sapmed.ac.jp.

[2] The abbreviations used are: ECM, extracellular matrix; CK, cytokeratin; EpCAM, epithelial cell adhesion molecule; HPPL, Hepatic Progenitor Cells Proliferating on Laminin; PECAM, platelet endothelial cell adhesion molecule; E, embryonic day; P, postnatal day; aPKC, atypical protein kinase C.

livers, α5-containing laminins, which are laminins 511 (α5β1γ1) and 521 (α5β2γ1), were strongly expressed in basal lamina underlying portal and central veins, hepatic arteries, and bile ducts, whereas in regenerating mouse liver after two-thirds partial hepatectomy, α1-containing laminin, which is laminin 111 (α1β1γ1), was transiently expressed in liver lobules. Furthermore, in the developing liver, the basal lamina including laminin was detected around the liver bud and also around bile ducts at a later stage in development (13). However, it has not been determined which laminin isoforms are expressed at different stages of liver organogenesis. We have reported previously that α1-containing laminin (laminin 111) is essential for the bipotential liver progenitor cell line HPPL to develop apicobasal polarity and cholangiocyte characteristics in three-dimensional culture (14). Although our results indicated that laminin was essential for liver epithelial cells to establish the polarity and lumen as cholangiocytes, it has remained unknown how HPPL receives signals from α1-containing laminin and which cells provide laminin *in vivo* during bile duct development.

Integrin, a heterodimer consisting of α and β chains, is a major receptor for ECM proteins including laminins. Among the subunits, β1 chain has been shown to be required for developing appropriate tissue structures both *in vivo* and *in vitro* (15–18). A recent study showed that β1 integrin could mediate distinct signals by associating with different α subunits during epithelial morphogenesis (19). However, it remains unknown which type of laminin isoform is important as a ligand for β1 integrin to regulate a specific step of epithelial tissue morphogenesis. Furthermore, the roles of β1 integrin in the formation of liver tissue architecture have not been studied yet.

In this study, we investigated the expression and function of laminin isoforms containing α1 and α5 chains in bile duct development. By using neutralizing antibody against β1 integrin and siRNA against laminin α5, we addressed the roles of these laminin isoforms in cyst morphogenesis in three-dimensional culture. We also addressed the roles of α1- and α5-containig laminins *in vivo* by demonstrating the normal emergence of cholangiocytes and the abnormal morphogenesis of bile ducts in laminin α5 knock-out mice. Our results indicate that liver epithelial cells sequentially utilize α1- and α5-containing laminins as ligands for β1 integrin in distinct processes of bile duct morphogenesis, revealing the functional significance of the transition from α1- to α5-containing laminin, which occurs widely in the basal lamina of developing epithelial tissues.

EXPERIMENTAL PROCEDURES

ECM Proteins and Growth Factors—Type I collagen was purchased from Koken Co., Ltd. (Tokyo, Japan). Growth factor-reduced Matrigel and purified laminin 111 were from BD Biosciences. Recombinant laminin 511 was produced in HEK293 cells triply transfected with mouse laminin α5, β1, and γ1 chains and purified as described previously (20). Epidermal growth factor (EGF) and hepatocyte growth factor were from Invitrogen and R&D Systems (Minneapolis, MN), respectively.

Culture of HPPL in Two- and Three-dimensional Conditions—HPPL was kept in DMEM/F-12 (Sigma) containing 10% FBS (Invitrogen), 1× insulin/transferrin/selenium (Invitrogen), 10 mM nicotinamide (Wako, Osaka, Japan), 0.1 μM dexamethasone (Sigma), 5 mM L-glutamine, and 5 ng/ml hepatocyte growth factor and EGF. To induce the formation of cyst structures, we modified the method reported previously (14). The bottom layer of culture was prepared in each well of 8-well coverglass chambers (Nunc, Roskilde, Denmark) by adding 50 μl of a 1:1 mixture of Matrigel and type I collagen solution. HPPL (3×10^3 cells in 150 μl of medium) was plated on the bottom layer. After 10 min of incubation, the cells were covered with 10% Matrigel in DMEM/F-12 containing growth factors. At day 4 of the culture, the upper layer of Matrigel was replaced with fresh DMEM/F-12 containing 5% Matrigel and growth factors.

Transfer of Cysts from Matrigel to Type I Collagen Gel—HPPL was kept in 5% Matrigel for 4 days in a well of a coverglass chamber to allow the cells to generate cyst structures. After washing with PBS, ice-cold Cell Recovery Solution (BD Biosciences) was added to the well. The chamber was put on ice for 1 h. The whole solution was transferred to a 15-ml tube and then centrifuged at 1,200 rpm for 4 min. The pellet containing cysts was resuspended in type I collagen solution and poured into a 1-cm-diameter tissue culture insert (0.02-μm Anopore membrane, Nunc). HPPL cysts were kept in type I collagen gel for 3 additional days before immunocytochemical analysis.

Blocking Interactions between HPPL and Laminins in Three-dimensional Culture—Neutralizing antibodies against β1 integrin (clone Ha2/5, BD Biosciences), α6 integrin (clone GoH3, Biolegend, San Diego, CA), and αV integrin (clone RMV-7, Biolegend) were used at a final concentration of 50 μg/ml to block the interaction between HPPL and ECM components. Hamster IgM (BD Biosciences) and rat IgG (Biolegend) were used as controls. Antibodies were added from the beginning or at day 4 of three-dimensional culture. Three thousand cells suspended in 150 μl of DMEM/F-12 containing growth factors were plated into each well of an 8-well coverglass chamber (Nunc) coated with a mixture of type I collagen and Matrigel. Ten minutes after plating, 150 μl of 10% Matrigel containing control IgM, control IgG, or neutralizing antibody was added and mixed by gently tapping. When antibody was added at day 4 of the culture, wells were added with 400 μl of ice-cold Cell Recovery Solution (BD Biosciences) and incubated on ice for 30 min. After washing with medium, 200 μl of fresh medium containing 5% Matrigel, growth factors, and IgM, IgG, or neutralizing antibody was added to each well.

Knockdown of Laminin α5—piLenti plasmids containing target sequences were purchased from Applied Biological Materials Inc. (Richmond, British Columbia, Canada). piLenti, pRev, and pGag plasmids were co-transfected into 293T cells. Culture medium containing lentivirus particles was diluted with fresh medium containing growth factors and added to HPPL. After 3 days, the medium was replaced with fresh medium containing 1 μg/ml puromycin. After selecting puromycin-resistant cells, the expression of laminin α5 was examined by quantitative PCR.

Culture of Hepatoblasts—Hepatoblasts were isolated from E14.5 liver based on expression of Dlk1 as reported previously (21). Cells were plated on dishes coated with either laminin 111 or recombinant laminin 511 and kept in the same medium used

TABLE 1
Primary antibodies used for immunostaining

Antigen	Company or source	Host	Dilution
E-cadherin	BD Transduction Laboratories	Mouse	1:1,500
β-Catenin	BD Transduction Laboratories	Mouse	1:1,500
Cytokeratin 19	Tanimizu *et al.* (21)	Rabbit	1:2,000
EpCAM	BD Pharmingen	Rabbit	1:500
α6 integrin	Biolegend	Rat	1:500
β1 integrin	Chemicon	Rat	1:500
β4 integrin	BD Pharmingen	Rat	1:500
HNF4α	Santa Cruz Biotechnology	Goat	1:200
Laminin α1	A gift from Dr. Takako Sasaki (Oregon Health and Science University)	Rabbit	1:2,000
Laminin α5	A gift from Dr. Takako Sasaki (Oregon Health and Science University)	Rabbit	1:2,000
Protein kinase ζ	Santa Cruz Biotechnology	Rabbit	1:100
Sox9	Millipore	Rabbit	1:500
ZO1	Zymed Laboratories Inc.	Rabbit	1:200
ZO1	A gift from Dr. Bruce Stevenson (University of Alberta)	Rat	1:2,000

for HPPL. After 3 days, the culture medium was replaced with serum-free DMEM/F-12 containing 500 pg/ml TGFβ. After 24 h of stimulation, cells were dissolved in a lysis buffer and used for RNA preparation.

Immunofluorescence Microscopy—Mouse embryonic and neonatal livers were fixed in PBS containing 4% paraformaldehyde at 4 °C, embedded in optical cutting temperature compound (OCT) compound, and frozen. Laminin α5 KO livers were kindly provided by Dr. Jeff H. Miner (Washington University, St. Louis, MO). They were used for preparation of thin sections using a cryostat (Leica, St. Gallen, Switzerland). Serial sections along the cranial tail axis were prepared from three homozygous mutant and two heterozygous livers. To count the number of duct structures and measure the lumen size, $CK19^+$ structures around the portal veins were examined in more than 10 sections at different locations along the axis from the liver hilum to the periphery. Samples of the culture were gently washed with PBS and then fixed in paraformaldehyde solution. After incubation in PFS (PBS containing 7% cold water fish gelatin (Sigma) and 0.1% saponin (Sigma)) at 4 °C for 30 min, primary antibodies diluted in PFS were added to each well. To remove excess antibodies, samples were gently washed with PBS. Primary antibodies used in this study are listed in Table 1. Signals were visualized with Alexa Fluor-conjugated secondary antibodies (Molecular Probes, Eugene, OR) used at a dilution of 1:500. F-actin bundles were detected with Alexa Fluor 488-, 555-, or 633-conjugated phalloidin (Molecular Probes) at a dilution of 1:250. Nuclei were counterstained with Hoechst 34580. Samples were examined using Zeiss LSM 510 and Olympus FV1000D IX81 confocal laser-scanning fluorescence microscopes.

Live Cell Imaging—HPPL expressing YFP-actin was kept in 5% Matrigel for 4 days in a 2-well coverglass chamber (Nunc). After exchanging the upper layer with fresh medium containing 5% Matrigel and either hamster IgM or anti-β1 integrin antibody (Ha2/5), the coverglass chamber was set on the stage of an Olympus FV1000 IX81 microscope. The temperature and CO_2 concentration were kept at 37 °C and 5%, respectively. Fifteen points were selected and followed for 24 h. Every 40 min, an X-Y image was captured at each point.

Cell Isolation and Quantitative PCR—E14.5 liver cells were labeled with FITC-conjugated rat monoclonal anti-Dlk1 (22), phycoerythrin-conjugated rat monoclonal anti-PECAM (Biolegend), allophycocyanin-conjugated rat monoclonal anti-p75NTR (23), allophycocyanin/Cy7-conjugated rat monoclonal anti-CD45 (Biolegend), and allophycocyanin/Cy7-conjugated rat monoclonal anti-TER119 (Biolegend) antibodies. E17.5 liver cells were labeled with FITC-conjugated rat monoclonal anti-EpCAM (24) and phycoerythrin-conjugated rat monoclonal anti-ICAM1 (BD Biosciences) antibodies. Postnatal day 0 (P0) liver cells and adult liver nonparenchymal cells were labeled with the FITC-conjugated anti-EpCAM antibody. Cells were fractionated on a FACSvantage SE or FACSAria (BD Biosciences). Isolated cells were used for RNA isolation followed by cDNA synthesis using Omniscript reverse transcriptase (Qiagen, Dusseldorf, Germany). PCR was performed on an ABI Prism 7500 (Applied Biosystems Inc., Foster City, CA) with TaqMan gene expression assays for mouse laminins α1 and α5 and hypoxanthine phosphoribosyltransferase. The threshold cycle (Ct) for each sample was determined on the ABI Prism software. We used the comparative Ct method to compare expression levels of laminin α chains among liver cell fractions using hypoxanthine phosphoribosyltransferase as an internal control and P0 kidney as a calibrator sample. The relative expression level was determined as the value of $2^{-\Delta\Delta Ct}$. ΔCt and ΔΔCt were determined by using the following formulas: ΔCt (a liver cell fraction) = Ct (laminin α1 or α5) − Ct (hypoxanthine phosphoribosyltransferase) and ΔΔCt = ΔCt (a liver cell fraction) − ΔCt (P0 kidney).

RESULTS

β1 Integrin Signal Is Necessary for Liver Progenitor Cells to Develop and Maintain the Cyst Structure—HPPL forms cysts with a central lumen in three-dimensional culture (14). Because β1 integrin was expressed at the basal domain of HPPL throughout cyst morphogenesis in culture (Fig. 1*A*), we considered the possibility that β1 integrin transmits signals from the ECM for liver progenitor cells to develop apicobasal polarity and lumen. To test whether the interaction between ECM and β1 integrin is required for the development of cyst structures, we used a neutralizing anti-β1 integrin monoclonal antibody (clone Ha2/5). The addition of the anti-β1 antibody from the beginning of three-dimensional culture (Fig. 1*B*) remarkably inhibited the lumen formation (Fig. 1*C*). In the control culture, HPPL formed cysts with polarity markers at their proper locations (Fig. 1*D*, *upper panels*); apical markers atypical protein kinase C (aPKC) (Fig. 1*D*, *panel 2*) and F-actin (Fig. 1*D*, *panel 3*) were localized at the apical membrane, whereas α6 integrin was

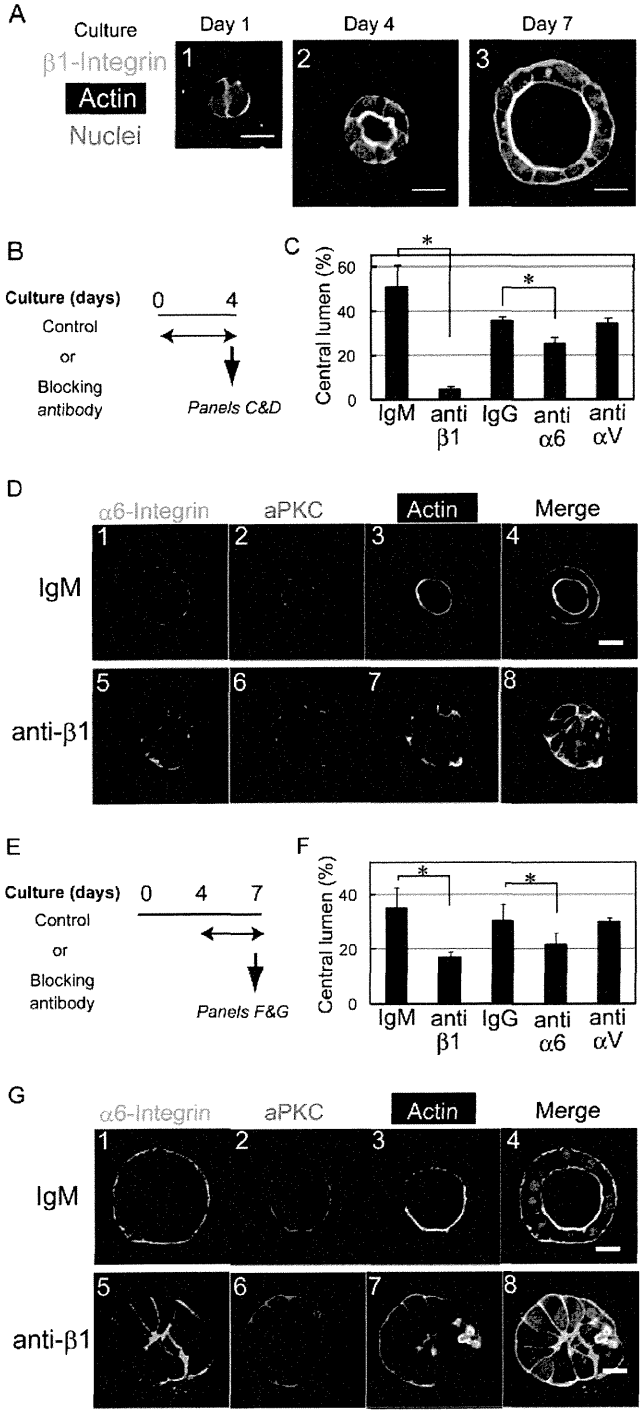

FIGURE 1. **β1 integrin is necessary for HPPL to develop and maintain the cyst structure.** *A*, expression of β1 integrins during three-dimensional culture. β1 integrin is clearly localized at the basolateral domain throughout the culture. Cysts were stained with anti-β1 integrin antibody, which was visualized with Alexa Fluor 488-conjugated anti-rat IgG and Alexa Fluor 633-conjugated phalloidin. The *bar* represents 20 μm. *B*, timetable for the addition of the anti-β1 integrin (clone Ha2/5), anti-α6 integrin (clone GoH3), or anti-αV integrin (clone RMV7) antibody to three-dimensional culture to examine roles of laminin-integrin interactions in the development of the cyst structure. One of those blocking antibodies was added to three-dimensional culture from the beginning, the lumen formation was examined as shown in *C*, and immunofluorescence analysis was performed at day 4 as shown in *D*. *C*, anti-β1 and -α6 antibodies decrease the number of cysts with a central lumen. The number of cellular structures with or without lumen was counted under a microscope. Cultures were repeated three times independently. More than 200 cellular structures in each well were examined. A *t* test was performed by Microsoft Excel software. *, $p < 0.05$. *D*, HPPL forms cell aggregates in the presence of the anti-β1 integrin antibody. In the control culture, aPKC (*D*, *panel 2*) and F-actin (*D*, *panel 3*) are localized at the apical domain, and α6 integrin (*D*, *panel 1*) is at the basolateral domains. In the presence of the anti-β1 antibody, aPKC (*D*, *panel 6*) and F-actin (*D*, *panel 7*) are localized at the boundary between cells and the ECM gel, whereas α6 integrin (*D*, *panel 5*) remains at the lateral domain but is excluded from the basal domain. *E*, timetable for the addition of the anti-β1, -α6, or -αV integrin monoclonal antibody to three-dimensional culture to examine the roles of the interaction in the maintenance of the cyst structure. One of the antibodies was added to three-dimensional culture at day 4, and the culture was terminated at day 7 for counting the number of cysts (*F*) and for immunofluorescence analysis (*G*). *F*, the number of cysts with a central lumen is decreased in the presence of anti-β1 or anti-α6 antibody. The number of cellular structures with or without lumen was counted at day 7 under a microscope. Cultures were repeated three times independently. More than 200 cellular structures in each well were examined. A *t* test was performed by Microsoft Excel software. *, $p < 0.05$. *G*, the cyst structure of HPPL is disrupted by the addition of the anti-β1 integrin antibody. aPKC (*G*, *panel 2*) and F-actin (*G*, *panel 3*) are localized at the apical domain, whereas α6 integrin (*G*, *panel 1*) is found at the basolateral domain in the control. By the addition of the anti-β1 antibody, the localization of aPKC (*G*, *panel 6*) and F-actin (*G*, *panel 7*) changes from the apical domain to near the ECM, whereas α6 integrin remains at the lateral domain but is excluded from the basal domain (*G*, *panel 5*). *Error bars* in *panels C* and *F* represent standard deviation. *Bars* represent 20 μm.

localized at the basal domain (Fig. 1*D*, *panel 1*). In contrast, in the presence of the anti-β1 antibody, HPPL formed cell aggregates without lumen (Fig. 1*D*, *lower panels*). In those cell aggregates, aPKC (Fig. 1*D*, *panel 6*) and F-actin (Fig. 1*D*, *panel 7*) were localized at the boundary between the cells and ECM. α6 integrin was localized at the cell-cell boundary but was absent at the boundary between cells and ECM (Fig. 1*D*, *panel 5*). We also added anti-α6 or anti-αV antibody to three-dimensional culture and found that anti-α6 antibody significantly inhibited the formation of cysts (Fig. 1*C*).

Next, to examine whether the β1 integrin signal is also important for maintaining the cyst structure, we added anti-β1 integrin antibody to the culture from day 4 of the culture and incubated it for an additional 3 days (Fig. 1*E*). Anti-β1 antibody reduced the number of cysts with a central lumen (Fig. 1*F*). Immunocytochemical analysis showed the altered localization of polarity markers in the presence of anti-β1 antibody; aPKC (Fig. 1*G*, *panel 6*) and F-actin bundles (Fig. 1*G*, *panel 7*) were localized at the boundary between the cells and ECM gel, whereas α6 integrin was excluded from the boundary (Fig. 1*G*, *panel 5*). We also added anti-α6 or anti-αV antibody to the culture from day 4 and found that anti-α6 antibody reduced the number of cysts (Fig. 1*F*).

β4 integrin, which is another β subunit expressed in HPPL, was detected at the basal surface of HPPL after the establishment of the apicobasal polarity (supplemental Fig. 1A). During the bile duct development, β4 integrin expression was observed from a later stage as compared with β1 integrin (supplemental Fig. 2). Based on these data, we considered the possibility that β4 integrin is involved in the maintenance of the cyst structure. We added a neutralizing antibody against β4 integrin from day 4 of the culture. The number of cysts was only slightly decreased in the presence of anti-β4 antibody (supplemental Fig. 1C), suggesting that it is not a major receptor mediating signals to HPPL for the maintenance of the cyst structure. These data indicated that the β1 integrin signal is required for

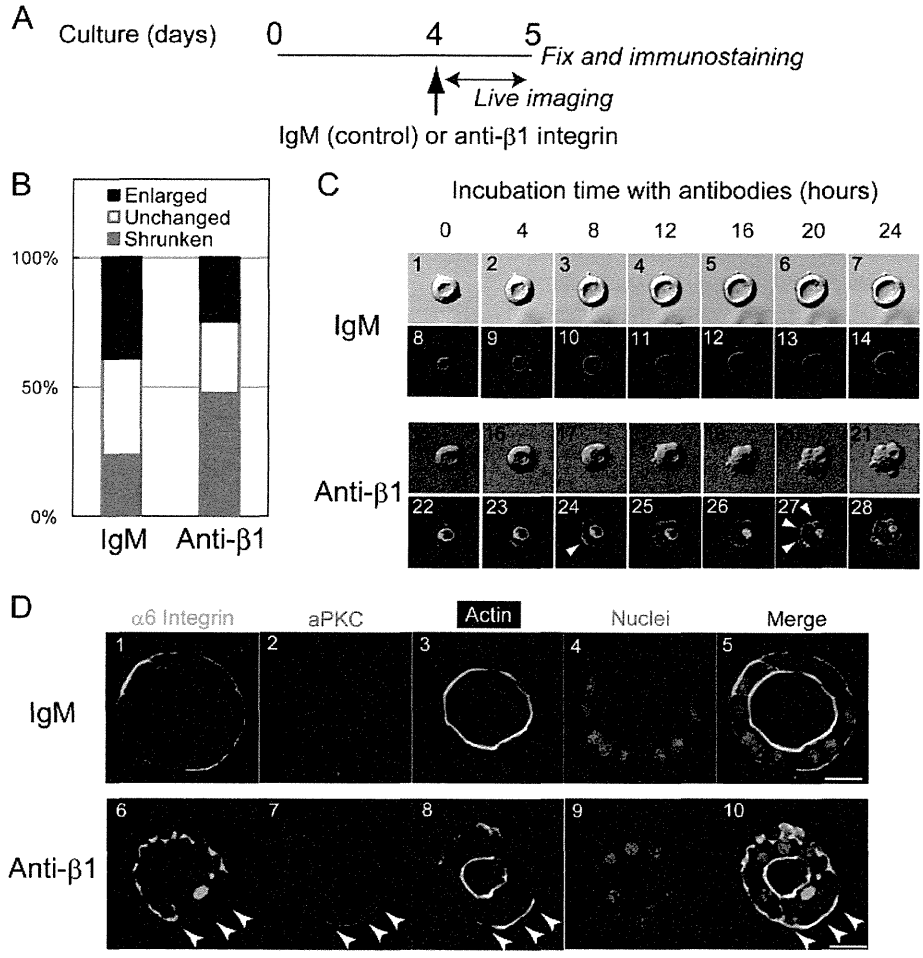

FIGURE 2. **Live cell imaging shows the processes of loss of normal polarity and collapse of the central lumen in the presence of anti-β1 integrin antibody.** *A*, timetable for live cell imaging and immunofluorescence. HPPL expressing YFP-actin was cultured in Matrigel for 4 days. After changing the upper layer to 5% Matrigel containing an anti-β1 integrin antibody, the plate was placed on a microscope, and images were acquired every 40 min in the following 24 h. *B*, the apical lumens of the cysts were categorized into three groups: enlarged, unchanged, and shrunken. The ratio of "shrunken" lumen was significantly increased in the presence of the anti-β1 integrin antibody as compared with the control. *C*, images taken every 4 h during live imaging are shown. Typically, HPPL exhibited a slightly expanded central lumen in the presence of control IgM (*panels 1–14*), whereas they lost apical localization of YFP-actin and the central lumen in the presence of the anti-β1 integrin antibody (*panels 15–28*). *D*, localization of apical and basal markers was examined at 24 h after the addition of the antibodies. When the central lumen still remained, apical markers such as aPKC and F-actin were evident at the basal domain (*D*, *panels 7* and *8*, *arrowheads*). In contrast, α6 integrin was excluded from the basal domain of the cells showing basal aPKC and F-actin (*D*, *panel 6*). *Scale bars* represent 20 μm.

both development and maintenance of the cyst structure and that α6 integrin is a crucial partner of β1 integrin.

Live Cell Imaging Shows a Link between Dissolution of Polarity and Collapse of the Central Lumen—The results using the anti-β1 integrin antibody showed that the interaction between β1 integrin and laminin is important for the maintenance of the cyst structure (Fig. 1*E*-G). However, immunofluorescence images at specific time points of three-dimensional culture did not reveal the entire picture of how blocking the laminin-integrin interaction disrupted the cyst structure. To visualize changes of the cyst structure by blocking the interaction between β1 integrin and laminin, a confocal microscope was used to monitor the cyst structure in three-dimensional culture for 24 h after the addition of the anti-β1 integrin antibody (Fig. 2*A*). Because F-actin bundles are an excellent indicator of polarity and lumen, we established HPPL cells expressing YFP-actin to visualize F-actin localization in live cells. We confirmed that YFP-actin was localized at the apical regions of cysts (Fig. 2*C*, *panels 8* and *22*). We monitored the size of the central lumen during incubation and classified the lumens into three types: enlarged, unchanged, and shrunken (or collapsed in some cases). Enlarged and shrunken cysts were observed most frequently in the absence and presence of the anti-β1 integrin antibody, respectively (Fig. 2*B*). Fig. 2*C*, *panels 1–14* (supplemental Movie 1) and *15–28* (supplemental Movie 2) show representative morphologies of enlarged and shrunken cysts in the presence and absence of anti-β1 integrin antibody, respectively. At 8 h after the addition of the antibody, YFP-actin appeared near the ECM (Fig. 2*C*, *panel 24*, *arrowhead*). At this time, the central lumen with an intense YFP-actin signal was still observed, although it had started to shrink. Beyond that time, basal actin became gradually evident (Fig. 2*C*, *panel 27*, *arrowheads*), and the lumen shrunk further and eventually collapsed. We then characterized cysts in culture by immunofluorescence staining at 24 h after the addition of the anti-β1 integrin antibody. At this time point, some cysts were still losing their polar-

ity and lumen. Even when the central lumen remained, aPKC and F-actin were localized near the ECM in some cells, whereas α6 integrin was excluded from the basal domain (Fig. 2*D*, *panels 6*, *7*, and *8*, *arrowheads*). These results suggested that the central lumen collapsed sequentially; at first, the interaction between laminin and β1 integrin was lost followed by dissolution of the apical proteins, and finally the central lumen collapsed.

Exogenous α1-containing Laminin Is Dispensable for Maintenance of the Cyst Structure—Because exogenous α1-containing laminin is needed for HPPL to form cysts (14), it was likely to be a major ligand for β1 integrin during the formation of cysts (Fig. 3*A*). However, it remained unknown whether exogenous α1-containing laminin is required after the formation of cysts. To address this question, we isolated cysts from Matrigel, the source of the α1-containing laminin, at day 4 and embedded them in type I collagen gel (Fig. 3*B*). Unexpectedly, even though α1-containing laminin was removed from the cysts (Fig. 3*C*, *panel 1*), the apicobasal polarity and the central lumen were maintained in the collagen gel (Fig. 3*C*, *panel 2*). This result indicated that exogenous α1-containing laminin was no longer required for the maintenance of the cyst structure, whereas β1 integrin signaling was required for the maintenance, suggesting that HPPL might produce laminins during cyst formation.

α5-containing Laminin Is Produced from HPPL and Integrated into an ECM Layer during Cyst Formation and Contributes to Expand the Lumen—To address the possibility that HPPL produces laminins, we examined the expression of laminin α chains in HPPL both in two-dimensional and three-dimensional culture conditions and found that HPPL expressed laminin α5 mRNA in both culture conditions (Fig. 3*D*). HPPL also expressed laminin β2 and γ1 chain mRNAs, indicating that the α5-containing laminin produced by HPPL was laminin 521. By immunostaining, we also examined whether HPPL expressed laminin α5 protein during cyst formation (Fig. 3*E*). At day 2 when the lumen was being developed, laminin α5 was detected at the boundary between the basal domain of cells and surrounding gel (Fig. 3*E*, *panels 1–4*). At day 4 when F-actin bundles lined the central lumen, laminin α5 was localized at the basal domain (Fig. 3*E*, *panels 5–8*). Basal laminin α5 was also observed at day 7 of culture (Fig. 3*E*, *panels 9–12*). These results suggested that α5-containing laminin was produced by HPPL and integrated into the ECM layer around cysts, contributing to the maintenance of the cyst structure.

To address the roles of α5-containing laminin in epithelial morphogenesis, we introduced siRNA against laminin α5 to HPPL and generated HPPL with reduced expression of laminin α5 (HPPL-siLamα5; supplemental Fig. 3). In three-dimensional culture, HPPL-siLamα5 formed cysts with a lumen, although the central lumen looked smaller than that of the control (Fig. 3*F*). We further measured the lumen diameter of cysts derived from HPPL-siLamα5 as well as those from the control. The result indicated that cysts derived from HPPL-siLamα5 had a significantly smaller lumen than those from the control at day 4 (Fig. 3*G*). Less extension of the apical membrane in HPPL-siLamα5 might be a reason for the formation of a smaller lumen (supplemental Fig. 4). These results suggested that endogenous α5-containing laminin is dispensable for establishing apico-

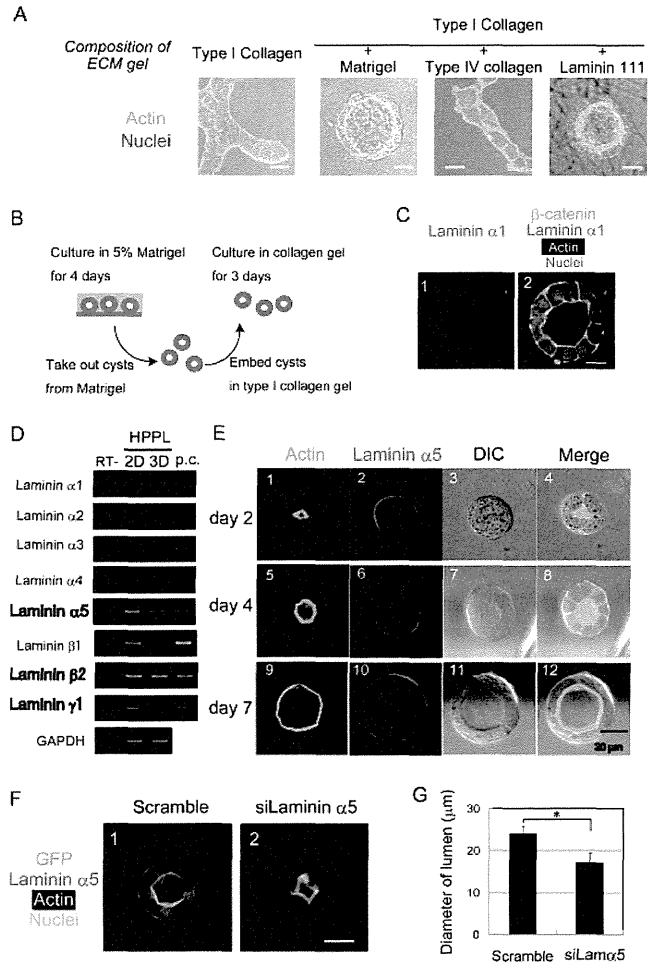

FIGURE 3. **HPPL produces α5-containing laminin.** *A*, HPPL forms cysts depending on laminin 111 (α1-containing laminin). HPPL was cultured in type I collagen gel or type I collagen gel containing 40% Matrigel, 40% type IV collagen, or 40% laminin 111. HPPL formed cysts in the presence of Matrigel or laminin 111. Cells were stained with Alexa Fluor 488-conjugated phalloidin and Hoechst 34580. *B*, a schematic view of the experiment to examine whether α1-containing laminin is crucial for HPPL to maintain the apicobasal polarity and lumen. HPPL was cultured in the presence of Matrigel for 4 days to form cysts. HPPL cysts were isolated from Matrigel by incubation in Cell Recovery Solution on ice for 1 h and then embedded in type I collagen gel. After incubation for 3 days in collagen gel, localization of β-catenin, laminin α1, and F-actin was examined. *C*, the cyst structure is maintained without exogenous α1-containing laminin. β-Catenin (*green*) and F-actin (*white*) are localized at the basolateral and apical domains, respectively, and the central lumen is maintained in type I collagen gel. The *bar* represents 20 μm. *D*, HPPL expresses laminins α5, β2 and γ1 in two-dimensional and three-dimensional culture. Expression of all the α chain, β1 and β2, and γ1 mRNAs was examined by RT-PCR. The α5, β2, and γ1 chains are expressed both in two-dimensional and three-dimensional culture, whereas the β1 chain is expressed in two-dimensional but not in three-dimensional culture. First strand cDNA synthesized from P8 kidney lysate was used as the positive control (*p.c.*). *E*, laminin α5 protein produced by HPPL accumulates at the basal surface of cysts. At day 2, F-actin is accumulated at the apical membrane of the developing central lumen. Laminin α5 is detected at the boundary between cells and Matrigel (*panels 1–4*). At days 4 and 7, HPPL cells develop an apical lumen surrounded by thick F-actin bundles, indicating that they have established apicobasal polarity. At these time points, laminin α5 is detected clearly at the basal surfaces of cysts (*panels 5–12*). *F* and *G*, HPPL-siLamα5 (HPPL expressing siRNA against laminin α5) forms smaller cysts as compared with the control. The control and HPPL-siLamα5 were cultured for 4 days. HPPL-siLamα5 forms a cyst with the central lumen surrounded by F-actin bundles (*white*), but the lumen size is smaller than that of the control cyst (*F*). The lumen diameter of cysts derived from HPPL-siLamα5 is statistically significantly shorter than that derived from the control HPPL (*G*). *Error bars* represent standard deviation. *DIC*, differential interference contrast.

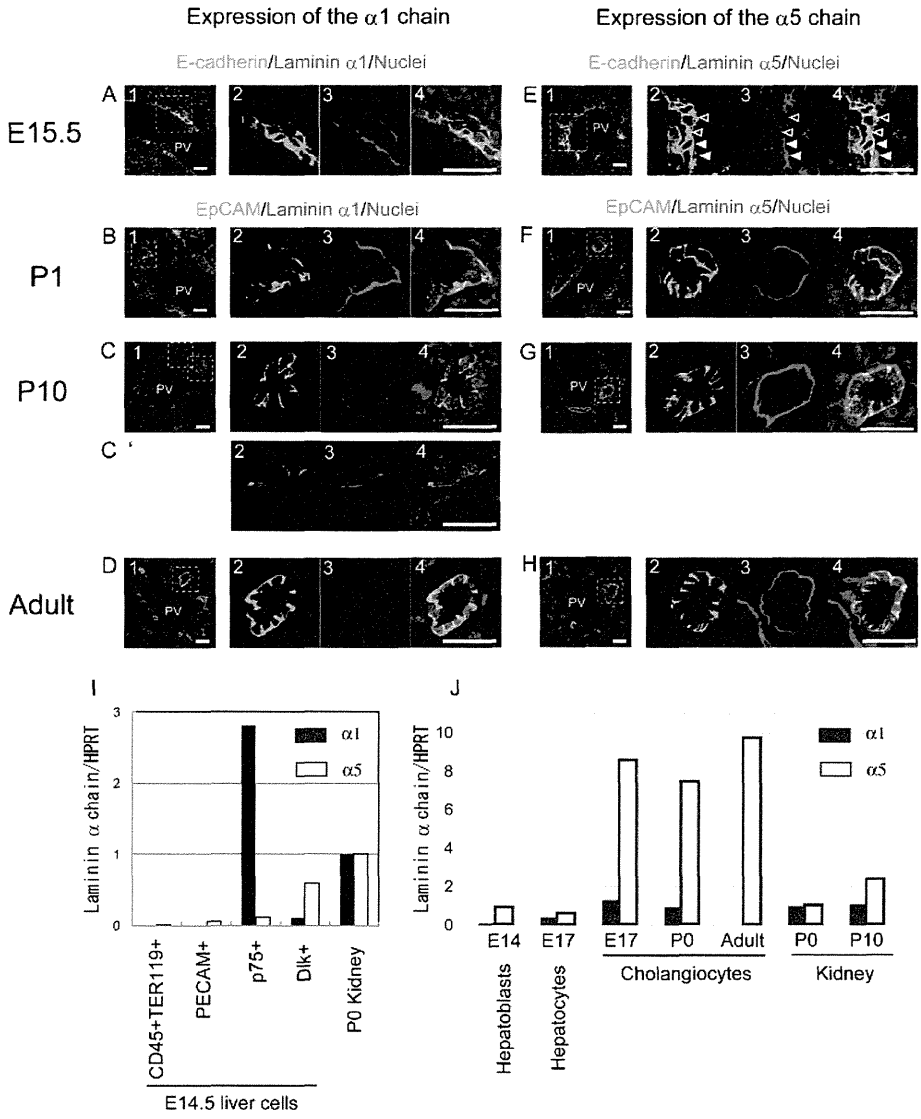

FIGURE 4. **Distribution of laminins α1 and α5 in developing liver.** *A–D*, laminin α1 is detected at the basal side of E-cadherin$^+$ cholangiocytes forming a ductal plate in E15.5 (*A, panels 1–4*) and EpCAM$^+$ cholangiocytes in the P1 liver (*B, panels 1–4*), whereas its expression is dramatically reduced in the P10 liver (*C, panels 1–4*) and then disappears from the basal side of cholangiocytes forming mature bile ducts in the adult liver (*D, panels 1–4*). In the P10 liver, α1 is still observed at the basal side of the remaining ductal plate (*C′, panels 2–4*). *Bars* represent 20 μm. *E–H*, laminin α5 is detected at the basal side of most of the E-cadherin$^+$ cholangiocytes in E15.5 (*E, panels 1–4*), although it is excluded from the basal side of some cholangiocytes (*open arrowheads*). In the P1 liver, laminin α5 is clearer at the basal side of cholangiocytes (*F, panels 1–4*). Later, laminin α5 is abundantly present at the basal side of cholangiocytes in P10 (*G, panels 1–4*) and adult liver (*H, panels 1–4*). *Bars* represent 20 μm. *I*, expression of laminins α1 and α5 by various types of cells at E14.5. Hematopoietic (CD45$^+$TER119$^+$) and endothelial (PECAM$^+$) cells, progenitors of stellate and periportal fibroblasts (p75NTR$^+$), and hepatoblasts (Dlk$^+$) were isolated from the E14.5 fetal liver when hepatoblasts near the portal vein were undergoing differentiation to cholangiocytes. p75NTR$^+$ cells express the α1 chain, whereas Dlk$^+$ cells weakly express the α5 chain. The levels of α1 and α5 chains are presented in this graph as the ratio against the expression level of each α chain in the P0 kidney. *J*, expression of laminins α1 and α5 during differentiation along the cholangiocyte lineage. Laminin α1 increased 5-fold in E17 cholangiocytes as compared with E14 hepatoblasts. However, the expression of laminin α1 mRNA was transient; it decreased in P1 cholangiocytes and then disappeared in adult cholangiocytes. On the other hand, laminin α5 increased 9-fold in E17 cholangiocytes as compared with E14 hepatoblasts, and the strong expression of laminin α5 was maintained in neonatal and adult cholangiocytes. The expression of α1 and α5 chains in Dlk$^+$ hepatoblasts, ICAM1$^+$ hepatocytes, and EpCAM$^+$ cholangiocytes isolated from the developing liver was examined by quantitative PCR. The levels of α1 and α5 chains are presented in the graph as the ratio against the expression level of each α chain in the P0 kidney. *HPRT*, hypoxanthine phosphoribosyltransferase; *PV*, portal vein.

basal polarity and lumen but does contribute to expand the apical lumen.

Expression of Laminins α1 and α5 in Vivo during Bile Duct Morphogenesis—It has been well established that cholangiocytes are associated with the laminin layer from the onset of their differentiation (13). However, it has remained unknown which laminin α chain is the major component at each specific developmental stage. We performed immunostaining of fetal, neonatal, and adult livers with antibodies against laminins α1 and α5 (Fig. 4). EpCAM staining clearly marks cholangiocytes beyond E17.5, and intensive E-cadherin staining at cell-cell contacts is a marker of newly differentiated cholangiocytes at E15.5 or E16.5 (3). At E15.5, laminin α1 was clearly detected at the basal side of E-cadherin$^+$ cholangiocytes in the ductal plate (Fig. 4*A*). Laminin α5 was also detected at the basal side of cholangiocytes (Fig. 4*E*, *closed arrowheads*). In contrast to